2010

Impervious Surfaces Mapping Using High Resolution Satellite Imagery

Tahmina Shirmeen

RAIN INDUCED RUNOFF SIMULATION USING A 2D NUMERICAL MODEL

A Thesis
presented in partial fulfillment of requirements
for the degree of Master of Science
at the National Center for Computational Hydroscience and Engineering
The University of Mississippi

by

TAHMINA SHIRMEEN

May 2016

ABSTRACT

Runoff plays an important role in the agricultural and urbanized environments. Surface runoff is determined primarily by the amount of precipitation and by infiltration characteristics related to soil type, soil moisture, antecedent rainfall, land cover type, impervious surfaces, and surface retention. In this study, CCHE2D, a numerical model for free surface flow hydrodynamics, is applied to study the rain induced runoff and channel flow mixed problems.

The main goal of this study is to incorporate rainfall as an input into the existing free surface flow model, CCHE2D; to verify and validate the CCHE2D model's runoff simulation capability using analytical solutions and experimental data so that the model is proven to be accurate and capable of simulating rainfall induced flow and runoff; and to simulate runoff process in complex watershed using high resolution data such as LiDAR topography to validate that the model can be applicable to problems with a variety of spatial scales and complexity.

Infiltration and subsurface flow is not considered throughout the study. The model's capability of simulating the rainfall generated runoff processes is tested using analytical solutions, experimental data and field data. Comparison of numerical solutions with both analytic solutions and observed overland flows resulting from unsteady rainfalls is satisfactory. To validate the applicability of the shallow water model CCHE2D, research has been conducted using very high resolution LiDAR data in a small real world agricultural watershed in northwestern Mississippi, USA, in the Mississippi River Alluvial Plain known as the Mississippi Delta. The fine resolution

of the numerical simulations resolved detailed runoff patterns in watersheds. This capability can be used for soil erosion and agro-pollutant transport and flood impact studies.

DEDICATION

This work is dedicated to my family.

LIST OF SYMBOLS

The following symbols are used in this research:

b = bed elevation (m);

C_m = coefficient (= 2.34375);

g = gravitational acceleration (m/s^2);

h = local water depth (m);

k = an exponent (= 5/3);

L = measured water surface elevation (m);

L_0 = measured water surface elevation at which the runoff starts after a rain (m);

n = Manning's roughness coefficient (m$^{-1/3}$s);

q = discharge of water per unit width (m^2/s);

Q = discharge of water (m^3/s);

R = rainfall intensity (L/T) (m/s, mm/h etc.);

S = friction slope;

T = rainfall duration (s);

t = time (s);

u = velocity component in the x direction (m/s);

u^* = shear velocity (m/s);

U = total velocity (m/s);

v = velocity component in the y direction (m/s);

Δx = mesh spacing in the runoff direction (m);

X = distance from the upstream boundary (m);

y = coefficient using in Formulated hydrograph (Eq. 25);

z = exponent using in Formulated hydrograph (Eq. 25);

α = depth-discharge coefficient (m^{2-k}/s);

η = water surface elevation (m);

ν = eddi viscosity coefficient (m^2/s);

κ = von Kármán constant (= 0.41);

ς = relative depth of the flow (m);

f_{cor} = Coriolis parameter;

$\tau_{xx}, \tau_{xy}, \tau_{yx}, \tau_{yy}$ = depth integrated Reynolds stresses and

τ_{bx}, τ_{by} = shear stresses on the bed (N/m^2).

ACKNOWLEDGEMNETS

I would like to express my sincere appreciation and thanks to my advisor, Dr. Yafei Jia for his thoughtful guidance, help, cooperation, and continuous encouragements throughout my graduate study in Computational Hydroscience and Engineering. My gratitude is extended to my thesis committee members: Dr. Mustafa Altinakar, Dr. Cristiane Q. Surbeck and Dr. Ron Bingner for their help, support and suggestions during this research.

My thanks are also due to Dr. Douglas Shields, Jr. for sharing research data and providing valuable insights for this work; Dr. Martin Locke and Dr. Richard Lizotte, Jr. for their valuable suggestions and help during this research; and Mark K. Griffith for his assistance in the field. I would like to thank all other faculty, scientists, and staff members at the National Center for Computational Hydroscience and Engineering for their help and support for my research.

This work was supported in part by the United States Department of Agriculture (USDA) Agriculture Research Service under the Specific Research Agreement No. 58-6408-1-609 monitored by the USDA-ARS National Sedimentation Laboratory and The University of Mississippi. I am very thankful to receive this support. My appreciation also goes to the School of Engineering, the University of Mississippi for the Thesis Fellowship Award. My special thanks are due to my husband Azad, my son Tamjeed, my daughter Zara, and all my other family members and friends without whose cooperation I couldn't complete this research.

TABLE OF CONTENTS

LIST OF TABLES

LIST OF FIGURES

CHAPTER 1

INTRODUCTION

1.1 Scope and Motivation

Runoff process is an important phenomenon in hydrology. Numerical modeling of runoff has a variety of applications in studying flood, soil erosion, water resources management, irrigation and ground water etc. With the advent of computer technology many numerical models have been developed based on different numerical approaches for different applications. In the past, the computational resources were limited; mostly one-dimensional (1D) flow models such as kinematic and diffusion wave approximations were used. Nowadays with the advances in numerical methods and computer technology, it is possible to solve this problem by using two-dimensional (2D) modeling approaches that solve the shallow water equations. These 2D approaches are capable of producing more detailed spatial representation of river channel and floodplain and have more applications for realistic problems (Marks and Bates, 2000).

The use of numerical modeling in planning, monitoring and managing is essential, which allows increase in understanding of water resources systems at different scales including water quantity and water quality issues. One of the most important advantages of modeling is that it saves time, lowers costs and allows to assess and manage potential water resources problems such as soil erosion and flood inundation etc.

Numerical modelling of runoff is often carried out using Digital Elevation Models (DEM) (Bates et al., 1997; Bates and Roo, 2000; Venkata et al., 2009). Runoff modeling has been reported normally using low resolution DEM data (grid size = 10 m x 10 m), which does not resolve small scale topographic features because of averaging the pixels in the data (Haile and Rientjes, 2005). The major disadvantage of using low resolution data is the inability to resolve small-scale features such as dikes, levees, ditches and culverts that block and affect flow patterns. With the developments in airborne remote sensing data capturing techniques such as LiDAR (Light Detection And Ranging), it is possible to obtain DEMs with higher resolution (grid size = 1.5 m x 1.5 m). In this research topographic features like roads, ditches and dikes are encountered. In the numerical simulations, high resolution LiDAR DEM data are used in order to analyze the detailed runoff patterns controlled by micro-rills and gullies generated from rainfall.

1.2 Research Goals and Objectives

The objectives of this thesis are listed as follows:

(1) to incorporate rainfall as an input into the existing free surface flow model, CCHE2D;

(2) to verify and validate the CCHE2D model's runoff simulation capability using analytical solutions and experimental data so that the model is proven to be accurate and capable of simulating rainfall induced flow and runoff;

(3) to simulate runoff process in complex watershed using high resolution data such as LiDAR topography to validate that the model can be applicable to problems with a variety of spatial scales and complexity. Of particular interest is how such high resolution DEM data can be used to model the micro topography and how it effects

the model results. The CCHE2D model is used to simulate runoff process in a watershed in the Mississippi River alluvial plain of northern Mississippi using LiDAR topographic data.

This thesis is organized as follows. First, a literature review of the numerical flow modeling is given in Chapter 2. Chapter 3 describes the two-dimensional hydrodynamic model, CCHE2D. Chapter 4 discusses verification and validation of the hydrodynamic model, CCHE2D, using analytical solutions and several available experimental cases. Chapter 5 presents the numerical model application to a real watershed. Finally, the conclusions and some suggested future work are discussed in Chapter 6.

CHAPTER 2

LITERATURE REVIEW

2.1 General Free Surface Flow Hydrodynamics

Numerical simulation has been increasingly used for studying overland flows in recent years. Many studies involving numerical modeling have been proposed and tested for modeling these flows (Liggett and Woolhiser, 1967; Cea et al., 2010; Kivva and Zheleznyak, 2005). The water flow is governed by the Saint-Venant (SV) equations under different conditions. Depending on the nature of the physical process, the governing equations of the flow can be simplified. The SV equations are coupled hyperbolic partial differential equations that are highly nonlinear and do not have general analytical solutions, therefore numerical methods must be used to solve them for realistic cases (Rousseau et al., 2012; Liggett and Woolhiser, 1967). Depending on the simplification of the momentum equations of the SV equations, three approaches are commonly used, fully dynamic wave model, diffusive (DW) model (Chow et al., 1988), and kinematic wave (KW) model (Singh, 2001; Singh, 2002; Morris and Woolhiser, 1980). Kinematic waves dominate the water flow when the inertial and pressure forces are negligible (Liu et al., 2004), while diffusive waves may be more applicable when pressure forces are important (Cea et al., 2010; Gottardi and Vinutelli, 2008). Dynamic wave approaches must be used when inertial and pressure forces and backwater effects are significant (Costabile et al., 2012).

Although overland flow could ideally be represented by the Saint-Venant equations, the kinematic solutions have been shown to yield very reliable results for most hydrologically

significant cases (Singh, 1996). Singh (1996) also mentioned that the kinematic wave modeling is gaining wide acceptance as a fast and accurate way to handle not only overland flow but also a wide range of watershed modeling problems. The kinematic approximation is the simplest, in which the friction slope is set equal to the bed slope (Book et al., 1982). In recent years, kinematic wave theory has been used successfully to describe overland flows (Woolhiser and Ligget, 1967; Freeze, 1978; Cundy and Tento, 1985). de Lima and Singh (2002) used a simple numerical model based on the non-linear kinematic waves that account for detailed, spatially distributed and dynamic representations of rainfall for comparing the results of hypothetical storms moving up and down on an impervious plane surface. Govindaraju, et al. (1990) developed analytical solutions using kinematic and diffusion wave approximations. Comparisons of analytical solutions of diffusion wave, kinematic wave, numerical solution of Saint-Venant equations and experimental data were discussed in this thesis. Esteves et al. (2000) solved the shallow water equations for runoff over an irregular topography of experimental scale with infiltration process considered. Henderson and Wooding (1964) used the kinematic wave equations for steady rain of finite duration and the runoff over a sloping plane. A comparison of the results of calculations with experimental measurements showed good agreements. The dynamic wave and diffusive wave models have been applied by Cea et al. (2010) to simulate runoff in several simplified urban geometries which have been tested in a laboratory rainfall simulator.

A number of numerical schemes have been proposed including the method of characteristics (Abbott, 1966), finite difference methods (Remson et al., 1971,) and finite element methods (Cooley and Moin, 1976, Fread, 1985, Szymkiewicz, 1991, 2012). Iwagaki (1955) provided one of the initial physical experiments for simulating rainfall-runoff processes involving three different slopes of laboratory flume, each subjected to different rainfall intensity. Morgali

and Linsley (1965) computed the overland flow generated by rainfall in a laboratory flume using a finite-difference one-dimensional shallow water model. Zhang and Cundy (1989) represent one of the fist attempts to model overland flow using the fully 2D shallow water equations; the authors used a finite-difference shallow water model to simulate one-dimensional rainfall experiments. Gottardi and Vinutelli, (2008) developed a two-dimensional finite difference runoff model by solving 2D Saint-Venant equations. By adopting the second-order Lax-Wendroff and three-point centered finite-difference schemes, they computed the simplified 1D and 2D overland flows by the kinematic wave and diffusive wave models and compared their numerical results with both analytical and experimental results by Morgali and Linsley (1965) and Govindaraju et al. (1990); their simulations showed that the simplified flow models can accurately predict the overland flow processes induced by steady and unsteady rainfall. Du et al. (2007) developed a distributed rainfall-runoff model using the one dimensional kinematic wave approximation solved by an implicit finite difference scheme. The flows in the channels are computed using a separate kinematic wave model. A two dimensional kinematic wave model was used by Liu et al. (2004) for simulating runoff generation and flow concentration using finite element method. Their comparisons with experimental observations with artificial rainfall were satisfactory.

Rousseau et al., (2012) developed finite volume and finite difference models for 2D Saint-Venant equations and Kinematic wave equations. Their tests indicated the finite volume version has a better performance than that of the finite difference. Nunoz-Carpena et al. (1993) solved kinematic wave equation using the Petrov-Galerkin method. Venkata et al. (2009) developed a Galerkin diffusion wave finite element model and applied to a small watershed. Jabar and Mohtar (2003) also develop a 2D kinematic wave finite element based overland flow model to study the overland flow.

2.2 Rainfall-Runoff Models for Events in Real World Watersheds

As overland flow or surface runoff is a dynamic part of the response of a watershed to the rainfall, modeling these situations leading to a number of numerical models based on different approximations to describe the flow. A number of proposed models and their performances discussed earlier only involved the ideal, experimental or test cases. It is important to analyze the models performance with a real world scenario along with real flood events. A number of simulations have been carried out using the different overland flow models initialized by the total rainfall.

Cea et al. (2008) simulated a real watershed in the region of Garcia, Northwest of Spain with a drainage area of 5 km^2 using a 2D shallow water model. Howes et al. (2006) modeled the overland flow generated by two different storms in two small rural semiarid watersheds (~2km^2) using a 2D model based on the kinematic wave approximation. The runoff hydrographs obtained with their numerical model showed good agreement with experimental results. Kivva and Zheleznyak (2005) modeled the rainfall–runoff in a small watershed area of Butenya river using a finite-difference shallow water model and found that their scheme is quite effective in analyzing such free-surface and moving boundary problem. Unami et al. (2009) used the 2D unsteady flow equations, solved with a finite volume method, to study the runoff processes in Northern Region of Ghanaian inland valleys. In their model particular attention is paid to achieve stable computation in complex topography. Costabile et al. (2012) solved the 2D shallow water equations using the finite volume method. The model was applied to study a real event in a small basin (40km^2) of Reno River, Italy. The resolution of the DEM was 20m. The overall result was satisfactory.

With the rainfall generated runoff term implemented into the existing CCHE2D hydrodynamic model, researches have been recently conducted to analyze the overland flow simulation capabilities and to simulate runoff in agricultural watersheds. In this study, the rainfall intensity is directly imposed in the hydrodynamic model as a source term, and a rating curve is imposed as a boundary condition at the watershed (channel) outlet. Depth-averaged Reynold's equations are solved in the model. Analytical and experimental studies are used to verify and validate numerical simulation results. In addition to overland runoff generated from the rainfall, this approach is capable of simulating both the overland runoff and channel flows. The CCHE2D model is finally used to simulate runoff in a watershed in the Mississippi River alluvial plain of northern Mississippi. This Mississippi Delta region is characterized by extremely deep, rich soils deposited through repeated flooding of the Mississippi River. This research utilized LiDAR-derived topographic data for this area. Processing of topographic data included land use land cover (LULC) distribution, soil distribution, hydrological analyses, and so on.

CHAPTER 3

NUMERICAL MODEL ENHANCEMENTS

3.1 CCHE2D Overview for Runoff Modeling

An existing shallow water flow model called the CCHE2D (Jia et al. 2002, 2013) is used for simulating the rainfall-runoff overland flow process. Figure 1 shows the definition sketch of problems to be studied in which the bed topography, the free surface flows and overland runoff are shown.

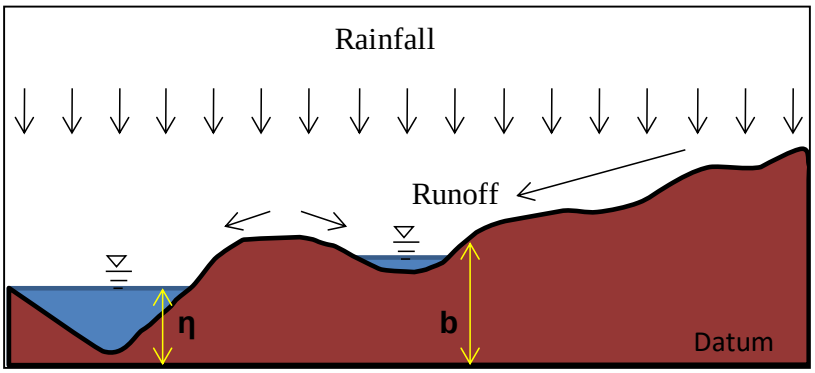

Figure 1. Definition sketch of the bed topography and the interested hydrologic processes, where, η = water surface elevation and b = bed elevation.

Surface runoff due to precipitation is a very shallow water flow. Therefore, it can be well represented by the 2D shallow water equations. In the shallow water studies, the St. Venant equation and its simplified versions, diffusion wave and kinematic wave equations, are generally employed. The depth integrated two-dimensional equations are generally accepted for studying

the open channel hydraulics. They have terms for turbulent stresses and uses to simulate mixed flow problems more realistically. CCHE2D is a hydrodynamic model for incompressible, free surface turbulent flows to simulate unsteady flows and sediment transport processes in channels, rivers, reservoirs, and around hydraulic structures. The numerical model CCHE2D is obtained by vertical integration of the 3D Reynolds averaged Navier-Stokes equations over the water depth. The model is a system of three partial differential equations with three unknowns defined in a 2D spatial domain. This section presents a brief description of the equations and schemes solved by the numerical model.

Free surface elevation of the flow is calculated by the depth integrated continuity equation in a Cartesian coordinate system as:

$$\frac{\partial h}{\partial t} + \frac{\partial uh}{\partial x} + \frac{\partial vh}{\partial y} = 0 \tag{1}$$

where h is the local water depth; u, v are depth-averaged velocity components in x and y directions respectively; t is the time. Because change in bed morphology is much slower process than hydrodynamics, free surface elevation of the flow, η, is calculated by the continuity equation as

$$\frac{\partial \eta}{\partial t} + \frac{\partial uh}{\partial x} + \frac{\partial vh}{\partial y} = 0 \tag{2}$$

For calculating the rain generated runoff, the rainfall intensity term, R, must be added as a source term in the continuity equation as

$$\frac{\partial \eta}{\partial t} + \frac{\partial uh}{\partial x} + \frac{\partial vh}{\partial y} = R \tag{3}$$

R may vary in time and space. The depth-integrated 2D momentum equations for turbulent flows are as follows:

$$\frac{\partial uh}{\partial t}+\frac{\partial uuh}{\partial x}+\frac{\partial vuh}{\partial y}=-gh\frac{\partial \eta}{\partial x}+\left(\frac{\partial h\tau_{xx}}{\partial x}+\frac{\partial h\tau_{xy}}{\partial y}\right)-\frac{\tau_{bx}}{\rho}+f_{Cor}v \tag{4}$$

$$\frac{\partial vh}{\partial t}+\frac{\partial uvh}{\partial x}+\frac{\partial vvh}{\partial y}=-gh\frac{\partial \eta}{\partial y}+\left(\frac{\partial h\tau_{yx}}{\partial x}+\frac{\partial h\tau_{yy}}{\partial y}\right)-\frac{\tau_{by}}{\rho}-f_{Cor}u \tag{5}$$

where g gravitational acceleration; $\tau_{xx},\tau_{xy},\tau_{yx},\tau_{yy}$ are depth averaged Reynolds stresses; τ_{bx},τ_{by} shear stresses on the bed, f_{Cor} is the Coriolis parameter. In the overland flow modeling, the Coriolis acceleration are neglected, the Reynolds stress terms are also ignored; making the equations 4 and 5 the shallow water equations.

In complex cases where runoff and channel flow conditions co-exist, a general flow model is necessary. The full forms of equations (3-5) make them applicable for general flow conditions. The Reynolds terms remain significant in the channel flow part of the domain. The turbulent Reynolds stresses in (Eq. 4 and 5) are approximated according to Boussinesq's assumption that they are related to the strains rate of the mean depth-averaged flow field with a coefficient of eddy viscosity:

$$\tau_{ij}=\nu_t\left(u_{ij}+u_{ji}\right) \tag{6}$$

where *i, j* represent *x* and *y* respectively and ν_t is the turbulent eddy viscosity. The CCHE2D model provides three kinds of closure models for eddy viscosity coefficient, i.e., the depth integrated parabolic eddy viscosity model, the depth integrated mixing length eddy viscosity model, and the depth integrated *k*-ε model (Jia and Wang, 1999; Jia et al. 2002). Throughout this study, the depth-integrated mixing length eddy viscosity model is used; which can be described as follows:

$$\nu_t = \bar{l}^2 \sqrt{2\left(\frac{\partial u}{\partial x}\right)^2 + 2\left(\frac{\partial v}{\partial y}\right)^2 + \left(\frac{\partial u}{\partial y} + \frac{\partial v}{\partial x}\right)^2 + \left(\frac{\overline{\partial U}}{\partial z}\right)^2} \tag{7}$$

In which

$$\bar{l} = \frac{1}{h}\int \kappa z \sqrt{\left(1 - \frac{z}{h}\right)} dz = \kappa h \int_0^1 \varsigma \sqrt{(1-\varsigma)} d\varsigma \approx 0.267 \kappa h \tag{8}$$

where κ = von Kármán constant (0.41) and ς is the relative depth of the flow and ν_t = eddy viscosity coefficient.

The depth-integrated velocity gradient along vertical coordinate $\frac{\overline{\partial U}}{\partial z}$ is introduced to account for the effect of turbulence generated from the bed surface. Assuming the flow is of logarithmic profile along the depth of the water. The depth averaged vertical gradient can be obtained by the following equation:

$$\frac{\overline{\partial U}}{\partial z} = C_m \frac{u^*}{\kappa h} \tag{9}$$

where u^* is the shear velocity and C_m is a coefficient assigned to be 2.34375.

A special finite element method called the efficient element method (Jia and Wang, 1999; Jia et al. 2002) is adopted in the model. The 2D shallow water equations are solved using a mixed finite element and finite volume method on a structured rectangular grid. The 2D finite-element model is discretized using nine-node quadrilateral elements. Partially staggered grid is used for solving these equations. In this model, a velocity correction method is used to couple the continuity equation and the momentum equations. Figure 2 shows the velocity and pressure location on a grid for calculation of the continuity equation. Because of the hydrostatic pressure assumption adopted

in the governing equations, the surface elevation plays the role of pressure fields. The continuity equation for surface elevation is solved on a staggered grid. Unsteady flow simulation is achieved by implicit scheme of time marching. The dry area method is used to handle the moving boundary of the unsteady flow.

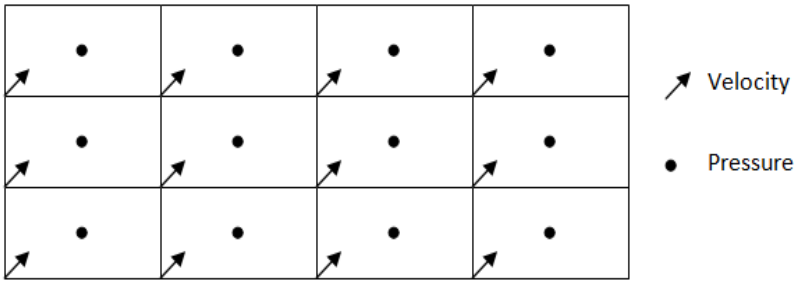

Figure 2. Velocity and pressure location on a grid for calculation of the continuity equation

3.2 Two-dimensional Kinematic Wave Model

Normally, a simplified version of Eqs. 3-5, the kinematic wave approximation, is used for runoff simulation. The kinematic wave approximation is one of the popular approximations to the full Saint-Venant equations in which the friction slope as well as water surface slope is equal to the bed slope. The water depth is very small and bed slope is parallel to the runoff slope, therefore one has

$$\frac{\partial \eta}{\partial x} \approx \frac{\partial b}{\partial x} \quad and \quad \frac{\partial \eta}{\partial y} \approx \frac{\partial b}{\partial y} \tag{10}$$

The turbulence stress terms in the momentum equations are also neglected because the dominant forcing for the overland flow is the gravity term, momentum advection and bed shear stress. Since shear stress of the overland flow is expressed as:

$$\tau = \gamma hS = \rho ghS \tag{11}$$

The flow velocity is estimated with the Manning's equation:

$$u = \frac{1}{n} h^{\frac{2}{3}} S^{\frac{1}{2}} \tag{12}$$

Shear stresses on the bed evaluated in conjunction with the Manning formula can be expressed as:

$$\tau_b = \frac{1}{h^{1/3}} \rho g n^2 U^2 \tag{13}$$

Or in the form of x-y components:

$$\tau_{bx} = \frac{1}{h^{1/3}} \rho g n^2 u U \quad \text{and} \quad \tau_{by} = \frac{1}{h^{1/3}} \rho g n^2 v U \tag{14 a, b}$$

For overland runoff, Eq. (4) and (5) are simplified to:

$$gh \frac{\partial \eta}{\partial x} = \frac{\tau_{bx}}{\rho} \quad \text{and} \quad gh \frac{\partial \eta}{\partial y} = \frac{\tau_{by}}{\rho} \tag{15 a, b}$$

where, h is the local water depth, n is the Manning's roughness coefficient, S is the slope, U is the total velocity and $U = \sqrt{u^2 + v^2}$.

Substituting Eq. 14 into Eq. 15 leads to the kinematic wave approximation (updated momentum equations) for the shallow water flows as

$$gh \frac{\partial \eta}{\partial x} = \frac{1}{h^{1/3}} g n^2 u \sqrt{u^2 + v^2} \tag{16}$$

$$gh \frac{\partial \eta}{\partial y} = \frac{1}{h^{1/3}} g n^2 v \sqrt{u^2 + v^2} \tag{17}$$

Equations (16 and 17) are still nonlinear, they can also be simplified from the Saint-Venant equations. Because the simplified kinematic wave model can only be applicable to the overland areas, Eqs. 3-5 are used in this study. CCHE2D model is in Fortran 90.

CHAPTER 4

MODEL VERIFICATION AND VALIDATION

In the numerical model development, verification is one of the most important steps, because one must assure that the numerical model is free of numerical errors in mathematical derivations and numerical formulations. For the validation of the numerical models, experimental data are needed. In this study the model verification was carried out using analytical solutions by Singh and Regl (1981) and Singh (1983). The numerical model was validated by reproducing experiments conducted by Cea et al. (2008), Morgali and Linsley (1965) and Govindaraju et al. (1990).

4.1 Model Verification using Analytical Solutions

Two analytical solutions were obtained by solving a one-dimensional kinematic equation analytically for rain generated runoff by Singh and Regl (1981) and Singh (1983). The solution of sustained rains for the runoff to reach a steady state (Singh and Regl, 1981) and solution for rainfall that stops before the runoff becomes steady (Singh, 1983), including the tailing stage solution after the rainfall stopped, were provided for obtaining their results. The governing one-dimensional kinematic equation for deriving these solutions reads:

$$\frac{\partial h}{\partial t} + u\frac{\partial h}{\partial x} = R \tag{18}$$

$$u = \alpha h^{k-1}; \quad q = uh = \alpha h^{k} \tag{19}$$

where q is the discharge of water per unit width (m^2/s), k is an exponent (=5/3) and α is a coefficient (m^{2-k}/s). Substituting Eq.(19) in Eq. (18), the kinematic-wave equation can be written as:

$$\frac{\partial h}{\partial t} + k\alpha h^{k-1}\frac{\partial h}{\partial x} = R \tag{20}$$

4.1.1 Initial and Boundary Condition Specifications

In addition to the above parameters, appropriate initial and boundary conditions should be specified for the mathematical model described in Eq. 18, 19 and 20. The kinematic wave approximation is applicable to runoff flow conditions. To solve the overland flows on a sloping plane subject to rainfall, initial dry bed conditions can be applied as:

$$h(x,0) = 0, \quad 0 \le x \le L \tag{21}$$

The upstream boundary condition is assumed as zero inflow, that is

$$u(0,t) = 0 \tag{22}$$

The upstream boundary condition for the runoff is one of zero depth, that is

$$h(0,t) = 0, \quad t \ge 0 \tag{23}$$

Here L is the length of the overland flow plane with a slope, x is the horizontal coordinate direction, t is the time. The rainfall intensity having a finite period of time can be expressed as:

$$R(x,t) = R > 0, \quad 0 \le t \le T;$$

$$R(x,t) = 0, \qquad t \ge T \tag{24}$$

where $T > 0$ is the duration of rainfall. These boundary and initial conditions are applicable not only for deriving analytical solutions, but also for numerical models to simulate analytical and experimental test cases. A rating curve, a relation between the water depth and the flow discharge for a particular case, is imposed at the downstream boundary. Table 1 shows the conditions of the analytical solutions of Singh and Regl (1981) and Singh (1983). Simulated results at several locations of the slope are presented in Figure 3 and Figure 4 respectively.

Table 1. Rain rate and conditions for analytical solutions

Solution	**Rainfall Intensity, *R* (m/s)**	**Coefficient, *α* (m^{2-k}/s)**	**Manning's, *n* ($m^{-1/3}s$)**	**Rain duration, *T* (s)**
1 Sustained rain	$2.7x10^{-5}$	5	0.02	1000
2 Short time rain	$2.7x10^{-5}$	5	0.02	200

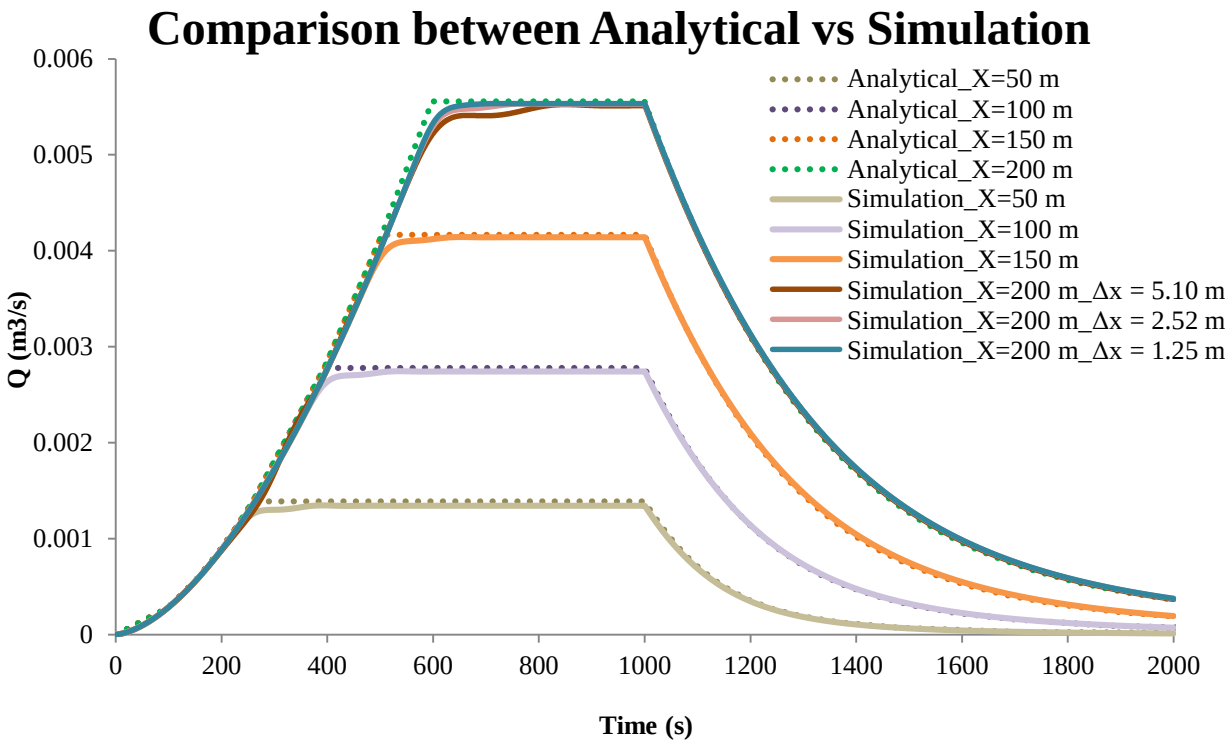

Figure 3. Runoff hydrograph for the analytical solution of the sustained rain followed by a falling limb and numerical solution by CCHE2D for rainfall of duration = 1000 s. Δx is the mesh spacing in the runoff direction.

Figure 3 shows the comparison of the simulated runoff and the analytical solutions collected at several locations: x = 50 m, 100 m, 150 m and 200 m from the upstream boundary of the runoff slope of 1.0%. Hydrographs at these fixed locations evolving in time are shown, and the equilibrium runoff (steady state) at each location is reached before the rain is stopped at T =1000 s. The runoff is always non-uniform. At first the flow is unsteady (rising limb), the flow then becomes steady until T =1000 s; it then becomes unsteady in the falling limb. The runoff reaches to equilibrium earlier at locations closer to upstream. The shape of the hydrograph is well predicted and matches well with the analytical solution. The simulated peak discharge is a little less than the analytic solution at the time of arrival.

It has been found that the mesh resolution affects the results slightly particular at the very downstream of the domain, and the solution can be improved by reducing the local mesh size effectively. The mesh was refined from coarser to finer mesh (Δx = 5.10 m to 1.25 m). Sustained rain solution (Figure 3) shows that discharge was underestimated at the outlet boundary (e. g. X = 200 m) when the mesh size was coarser. Finer (Δx = 1.25) grids show better agreement than the courser grids (Δx =5.10 m) at the outlet of X = 200 m.

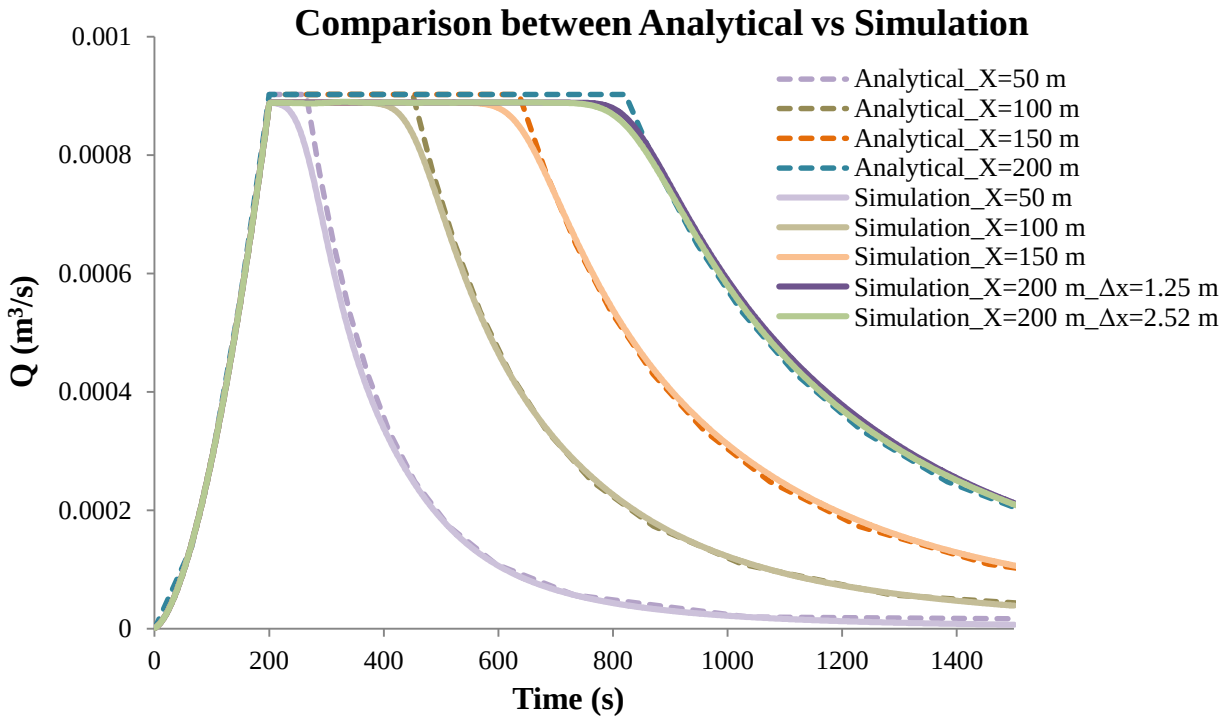

Figure 4. Runoff hydrograph for the analytical solution for short rain and numerical solution by CCHE2D for rainfall event with duration = 200 s. Δx is the mesh spacing in the runoff direction.

The short rain solution (Figure 4) is for cases in which the rain stops before a steady runoff is formed for the rain over a slope and the hydrographs have a different pattern from that of

sustained rain solutions. The peak discharge is the same for all locations because the flows at the downstream locations are sustained by those from upstream. At the time the rain stopped, the steady state conditions were attained at all locations for a short time period by those from upstream. Runoff recession is much earlier for the locations closer to upstream. The shape of the simulated hydrographs at all locations corresponded well with the analytical solutions.

4.2 Model Validation using Experimental Case Studies and Other Numerical Approaches

The numerical model was tested using several available laboratory experiments. All of these cases were carried out on impervious overland flow planes. The only variable measured in all of the experiments was the downstream runoff hydrograph.

4.2.1 Case 1

Morgali and Linsley (1965) obtained experimental runoff data. Their tests were carried out in a straight turf which was 21.945 m long with a unit width; the rain was uniform for 20 minutes. Parameters involved in these two experiments are described in Table 2 (Case 1A, 1B).

Table 2. Rain rate and conditions for Case 1

Test Case	***Slope (S)***	***n* ($m^{-1/3}$ s)**	***R* (m/s)**
1A	0.04	0.5	2.54×10^{-5}
1B	0.04	0.5	1.33×10^{-5}

A 110 x 10 uniform mesh and 0.01 s time step were used for the numerical simulation. It was found that these simple runoff experiments fit well with the analytical solution of Singh and

Regl (1981) as well as the experimental results (Figure 5). The rising limb of the discharge hydrograph and the peak discharge were captured very well by the simulations. Both curves (1A and 1B) look similar because the only difference in the experiment was rainfall intensity.

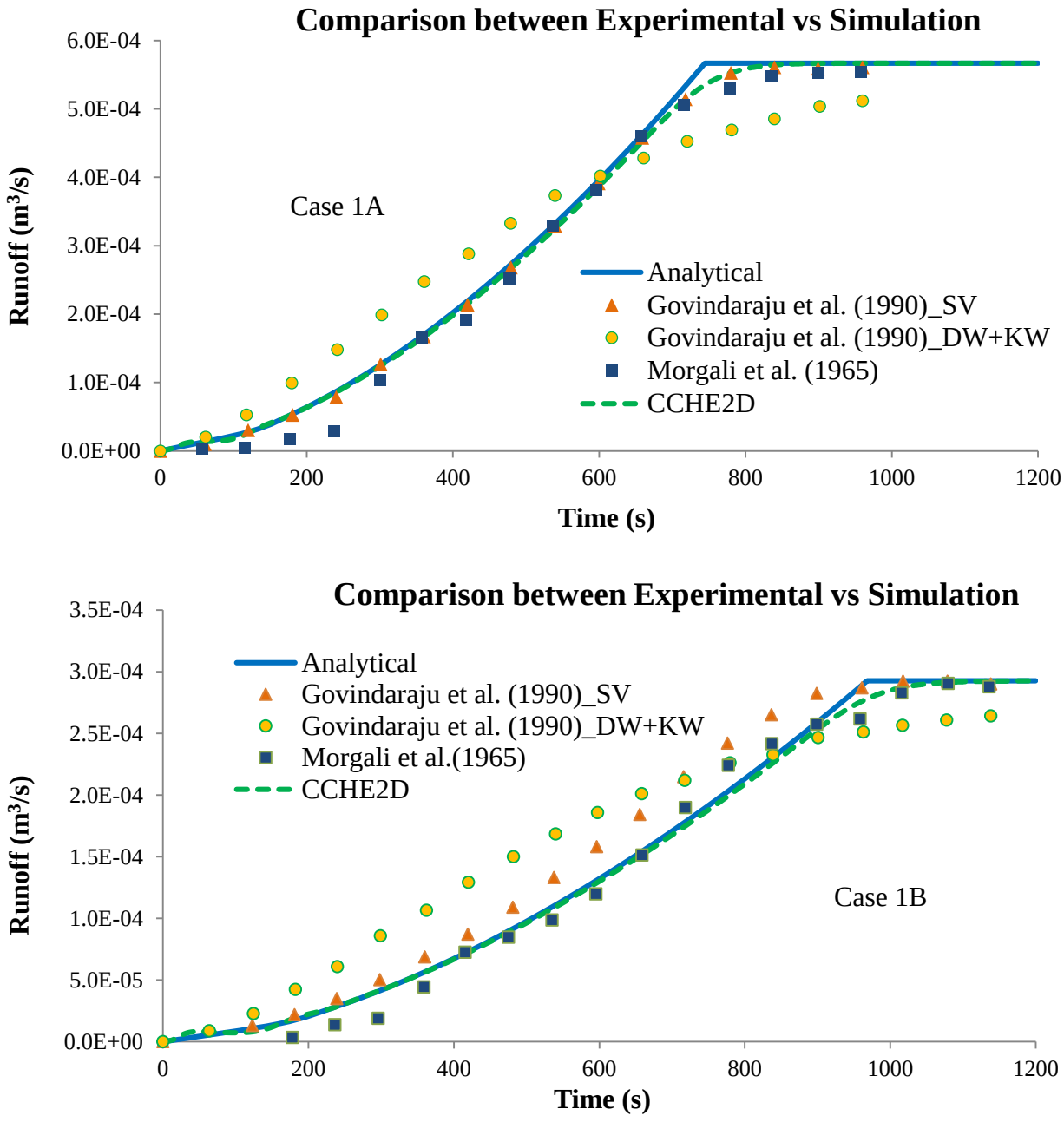

Figure 5. Comparisons of measured data with analytical solutions and numerical solutions

For both cases, the simulated arrival time of the maximum discharge showed good agreement with the analytical solution as well as the experimental data (Figure 5). The peak discharge of the experiments occurred at approximately 850 and 1100 s respectively for Case 1A and Case 1B. The numerical solutions of CCHE2D agreed well with the experimental data for both cases but the arrival times of the data are later that those given by the analytical solution. Figure 5 also compares the simulation result of Saint-Venant (SV) equations by Govindaraju et al. (1990); it is seen that the numerical solution based on the Saint Venant equations agreed well for the case with the higher rain, but the solution did not fit well for the case with the smaller intensity rainfall. Figure 5 also illustrates the semi-analytical Diffusion-wave (DW) and the Kinematic wave (KW) solutions of Govindaraju et al. (1990). The results of CCHE2D outperform this semi-analytical approximate solution.

4.2.2 Case 2

Cea et al. (2008) conducted runoff experiments of complex topography and simulated these cases using a 2D numerical model. The runoff experiments of Cea et al. (2008) were on an artificial rectangular watershed (2 m x 2.5 m) made by three planes of stainless steel, each of them with a slope of 0.05. Two dikes were set in the watershed to adjust the runoff direction and distribution. These dikes were placed in the watershed to vary the topography and the pattern of the runoff hydrograph. The length of the two dikes were 1.86 m and 1.01 m. The runoff accumulates and becomes channel flows along intercepting lines of slopes and dikes. These are the cases that can be handled only by hydrodynamic models solving full governing equations. The rains for the three tests of this case are different. In the first test (2A), rainfall intensity was 317 mm/h for 45 s. In the second test (2B), rainfall intensity was 320 mm/h for 25 s, it stops for 4 s and restarts for additional

25 s with the same intensity. In the third test (2C) rainfall intensity was 328 mm/h. The rain was set for 25 s; it stopped 7 s, and then restarted for another 25 s. Cea et al. (2008) simulated these tests with a two-dimensional unstructured finite volume model. In this study CCHE2D was applied and the numerical results were compared with experimental data. Table 3 shows the parameters for three laboratory experiments.

Table 3. Rain and watershed conditions (Cea et al. 2008).

Case 2	***S***	***n* ($m^{-1/3}$ s)**	***R* (mm/hr)**	***T* (s)**
2A	0.05	0.009	317	(0, 45)
			0	> 45
2B	0.05	0.009	320	(0, 25)
			0	(25, 29)
			320	(29, 54)
			0	> 54
2C	0.05	0.009	328	(0, 25)
			0	(25, 32)
			328	(32, 57)
			0	> 57

The watershed (Figure 6) was modeled using an irregular structured mesh with the cell size being in the range of 0.034 m to 0.009 m; the mesh spacing is refined near the main channel and the outlet for improving the results. Manning's roughness was set equal to 0.009 $m^{-1/3}$s. Numerical simulation time step 0.01s and the simulation time 120 s were assigned. In this case the channel flow and runoff were mixed: the runoff from the watershed surface was accumulated in the triangle shaped channel formed by the side slopes. Three different rainfall distributions were simulated and indicated in Figs. 7, 8 and 9 as Case 2A, 2B and 2C, respectively. The simulation results of Cea et al. (2008) are also presented in the Figures 7, 8, and 9 with those of this study.

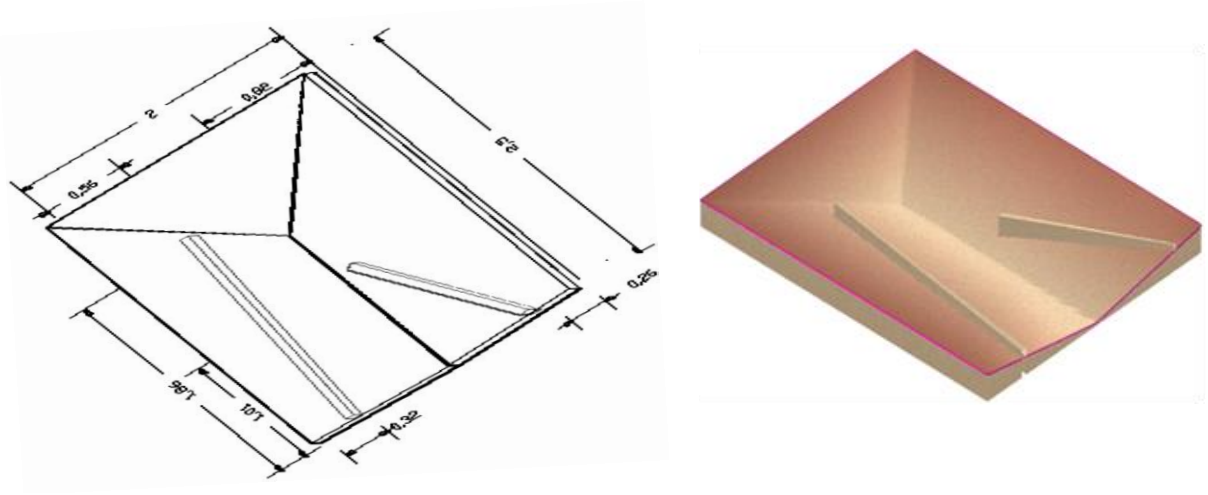

Figure 6. Experimental setup (left) and 3D view of the geometry (right), Cea et al., (2008). The scales are in meter.

4.2.2.1 Case 2A

Figure 7 shows the comparison between the numerical solution and experimentally observed runoff hydrograph. The solution of the CCHE2D model agrees very well with the experimental results. The flow discharge increased continuously once the rain started. The peak discharge occurred at the time the rainfall stops at 45 s. Although the rise and the fall limb of the hydrograph were slightly overestimated, the shape of the hydrograph and the peak discharge were predicted well.

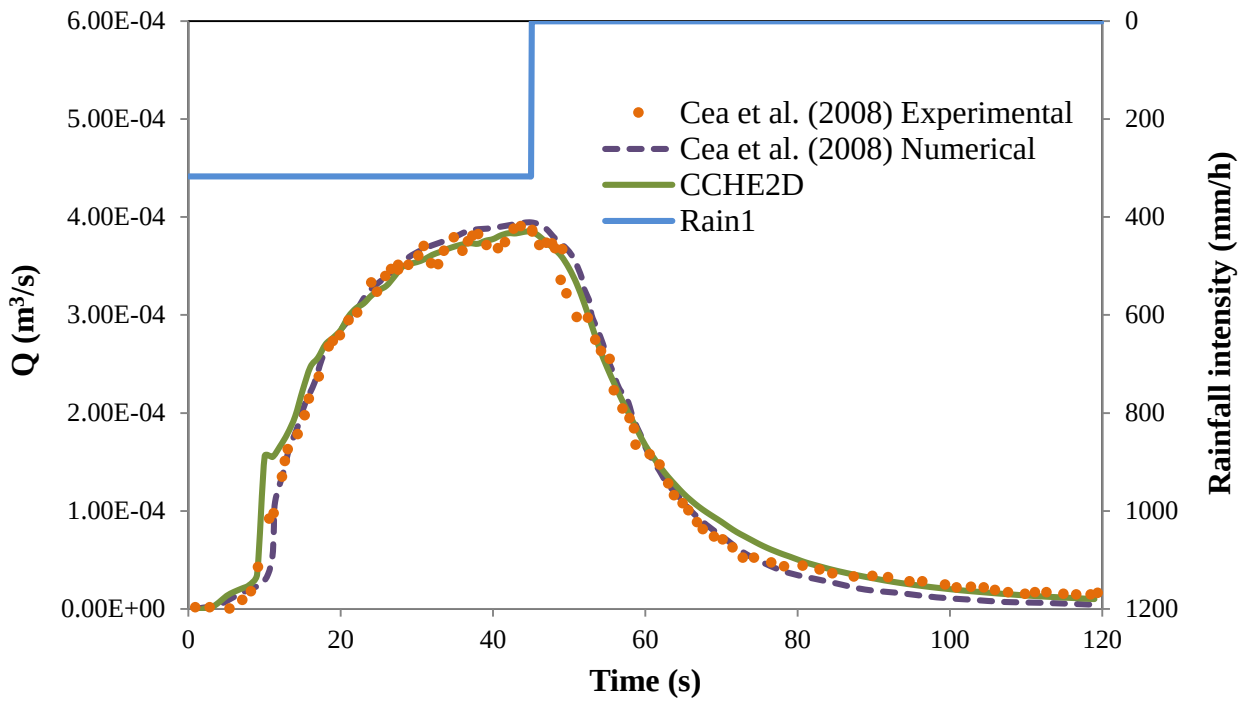

Figure 7. Comparison of simulated runoff hydrograph and experiment data of Case 2A

4.2.2.2 Case 2B

Figure 8 shows the comparison for Case 2B. In this case the shape of the overall runoff hydrograph was well predicted. Both of the peak discharges were predicted reasonably. The first peak discharge occurred when the rainfall stopped temporarily at 25 s. At that point the discharge started to decrease and continued to decrease for approximately 6 additional seconds after the rain restarted. This is because the runoff had a phase delay to the rain: it took some time for the runoff to reach the outlet boundary. The second peak discharge occurred at approximately 54 s. The falling limb of the hydrograph was slightly underestimated compared to the experimental data. The phase shift was also observed in the simulation result of Cea et al. (2008). Cea et al. (2008) indicated that the nozzle for generating the rainfall leaked for a while after the rain stopped, adding

extra water to the tail hydrograph. This additional water was not included in the rainfall and thus resulted in the phase shift that was also observed in the simulation result of Cea et al. (2008).

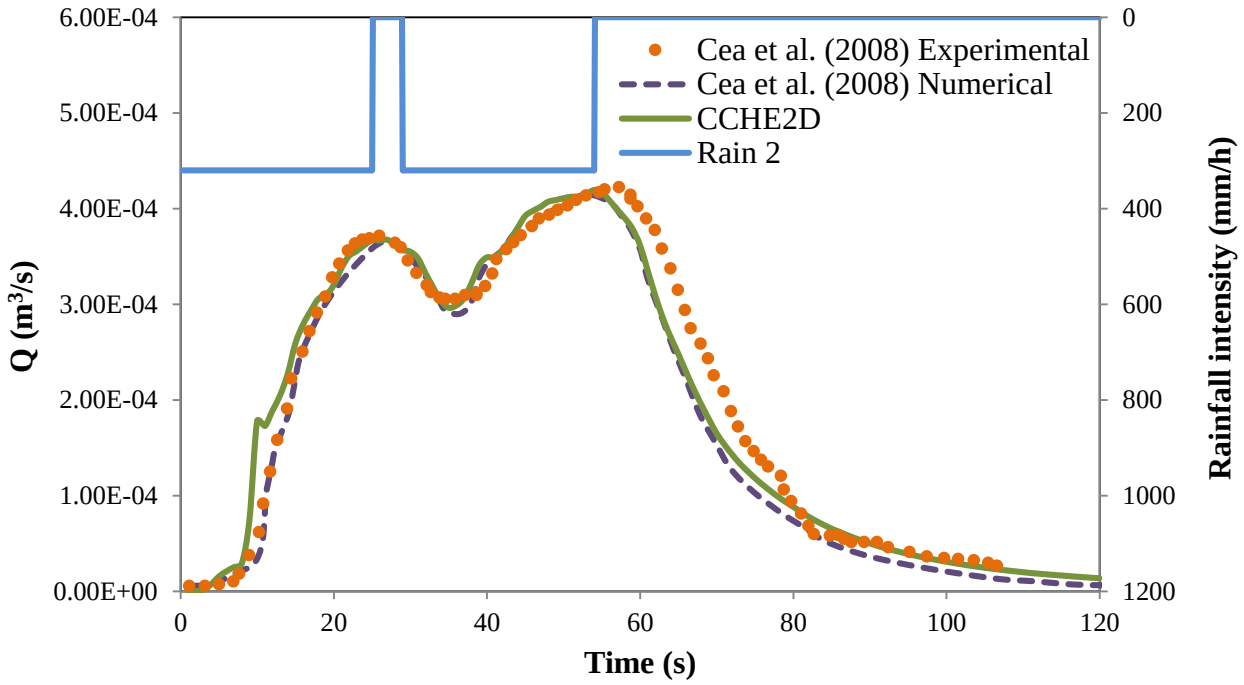

Figure 8. Comparison of simulated runoff hydrograph and experiment data of Case 2B

4.2.2.3 Case 2C

Figure 9 shows the comparison between the numerical and experimental runoff hydrograph of Case 2C. For this test case, the simulated processes and the observed physical processes showed good agreement. The shape of the hydrograph was well predicted too. The interval between the two rain peaks was 7 s. The first runoff peak discharge occurred at the time the rainfall stopped at 25 s. The runoff discharge decreased for approximately 10 s and then increased. The second runoff peak discharge occurred at approximately 57 s. Although the simulated runoff peak discharge was slightly underestimated, it well matched with the Cea et al. (2008) model results.

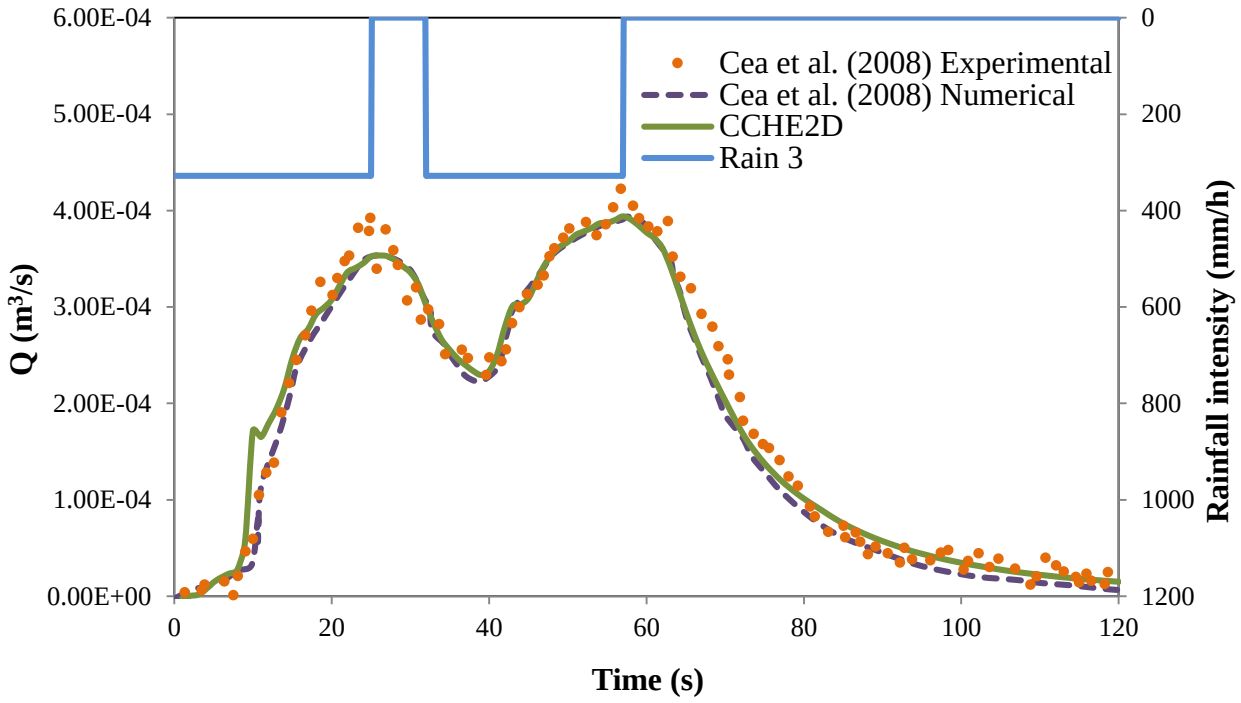

Figure 9. Comparison of simulated runoff hydrograph and experiment data of Case 2C

Figure 10 shows the simulated runoff unit discharge and water depth distributions in the experimental watershed at t = 24 seconds. Velocity vectors are indicated along with the unit discharge and the computational mesh is shown along with the water depth in the figure. The distributions indicate how the overland runoff accumulates toward the channel, affected by topography, dikes and discharged out of the watershed. The flows over the slopes are sheet runoff, but they become free surface flows with recirculation in the main channel. These flows cannot be represented by simply using a kinematic wave model.

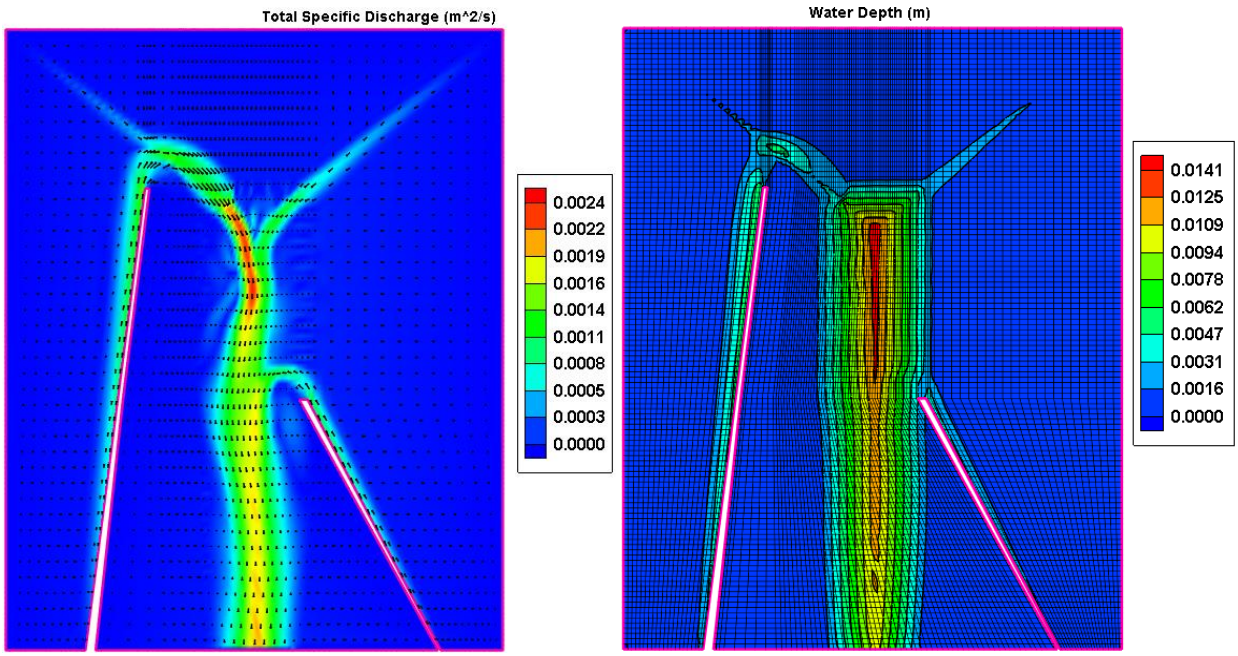

Figure 10**.** Simulated runoff unit discharge and vector distribution (left) and mesh and water depth distribution (right) at t = 24 s

CHAPTER 5

MODEL APPLICATION TO A REAL WORLD WATERSHED

This section involves overland runoff modeling due to rainfall using very high resolution LiDAR data in Howden Lake watershed which is situated in Bolivar County in the Mississippi Delta Region. No numerical study has been done before in this area. Howden Lake watershed represents a typical flat agricultural watershed in the Mississippi delta. Figure 11 shows the location and the aerial photography of the Howden Lake watershed. The watershed has an area of approximately 18 km^2.

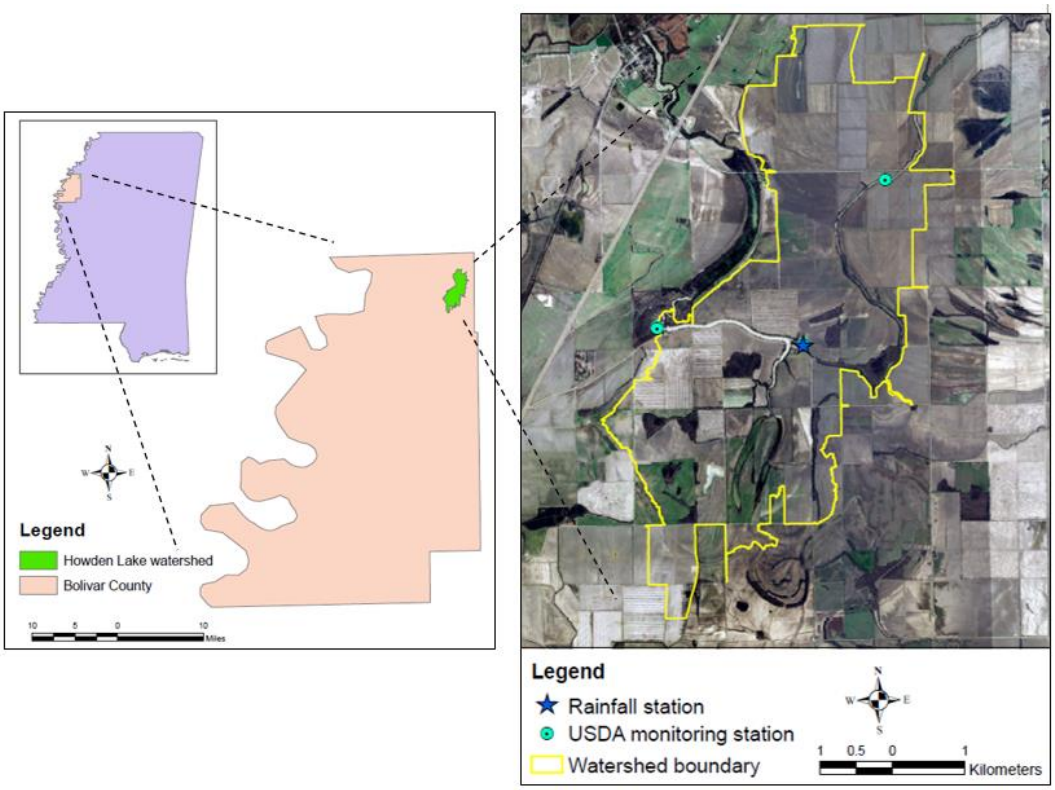

Figure 11: Location and Aerial photography of the Howden Lake watershed

5.1 CCHE2D Model Inputs

5.1.1 Topographic Data

USGS DEMs are commonly available to the public but their resolution (10 m^2) may be too coarse for this study. A more detailed topography of the studied watershed based on airborne LiDAR measurements was obtained from the United States Department of Agriculture (USDA) National Sedimentation Laboratory (NSL). The datasets were in ASCII format. Approximate horizontal resolution of this LiDAR data was 1.5 m. The original projected coordinate system was NAD 1983 State plane Mississippi West FIPS 2302 Feet. These datasets were re-projected to the dataset NAD 1983 UTM Zone15 N in meter using ArcGIS.

The collected LiDAR ASCII format data were used to prepare the mesh directly in the CCHE MESH Generator. Aerial photography and/or satellite imagery was obtained from NSL which also helped to reduce the human error for interpretation of the actual condition of the ground. The DEM data need to be subset using the watershed boundary before analyzing the watershed relief. Watershed boundary was also collected from NSL. The watershed elevation ranges from approximately 44 m to 48.8 m. Slope was determined within the GIS software by comparing the elevation of a grid cell with respect to the elevation of the neighboring grid cells. In most of the places the slope ranges from (0-3) degrees. Near the bank of a channel the slope was higher, ranges from (3-12) degrees. Table 4 shows the watershed areas, perimeter and relief for the entire watershed which is calculated using ArcGIS.

Table 4: Howden Lake (entire) watershed characteristics

Watershed perimeter (m)	Watershed area (m^2)	Watershed relief (m)	
		Max	Min
37966.84	17516395.18	48.8	44.8

5.1.2 Rainfall Data

Precipitation is one of the important parameters for the runoff overland flow modeling. The average annual precipitation in this region is about 1440 mm. There is only one rainfall station present in this area, established by the NSL (Figure 11). Several recorded large rain events provided by NSL were selected for the model application. These events are April 26-28, 2011; September 25-27, 2011; November 21-25, 2011; May 20-24, 2013; and October 30 - November 4, 2013. Figure 12 shows these rainfall events used for runoff simulation of the watershed. Among these events, 4/2011, 9/2011 and 10/2013-11/2013 were single-peaked (one major peak) rains, while those of 11/2011 and 5/2013 were double peaked (two major peaks). From the precipitation data it was found that the highest rainfall peak for 4/2011, 9/2011, 11/2011, 5/2013 and 10/2013-11/2013 rain storm events was approximately 23 mm, 20 mm, 10 mm, 8 mm and 7 mm respectively and the average peak rainfall intensity for 4/2011, 9/2011, 11/2011, 5/2013 and 10/2013-11/2013 storm events was 23.13 mm/hr, 3.74 mm/hr, 5.23 mm/hr, 6.29 mm/hr and 3.76 mm/hr respectively.

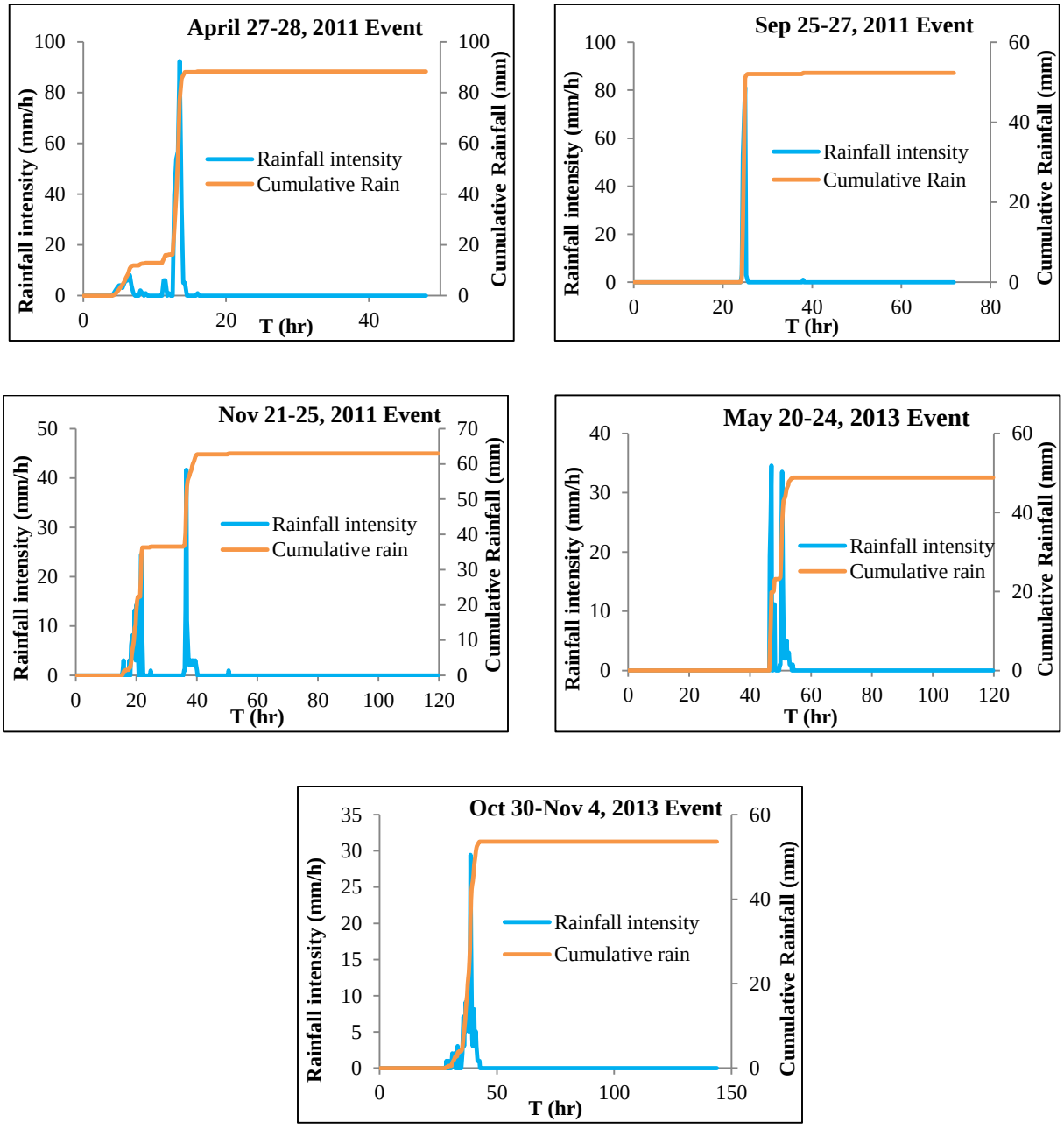

Figure 12: Rainfall events provided by NSL

5.1.3 Water Surface Elevation Data

Three monitoring stations were established and monitored by NSL in the entire watershed (Figure 11). Water surface elevation data was collected by NSL. We were particularly interested in the upstream sub-watershed where monitoring station 1 is situated (Figure 15). Flow stage data for this watershed were measured by field instrumentation. The gage station recorded the water surface elevation at regular time intervals. The flow discharge was not measured directly. In the absence of a well-developed rating curve for the monitoring station, water discharge was calculated from measured stage records by a power function of observed water stage data which is described later.

5.1.4 Soil Data

Soil type data was downloaded from Soil Survey Geographic (SSURGO) database to analyze the soil type distribution and prepare the soil map for the Howden Lake watershed. Figure 13 shows the soil map for this watershed. According to the soil map the watershed primarily consists of clayey soils (Alligator clay nearly level phase) which impedes infiltration.

Fisk (1944) described that the Mississippi River valley alluvial aquifer overlain by a capping layer, called the topstratum, is a combination of sand, silts and clays comprising a relatively impervious layer. Infiltration was therefore considered to be minimal and was not included in the simulation. The area near the channel was also mostly clay with gently sloping phase.

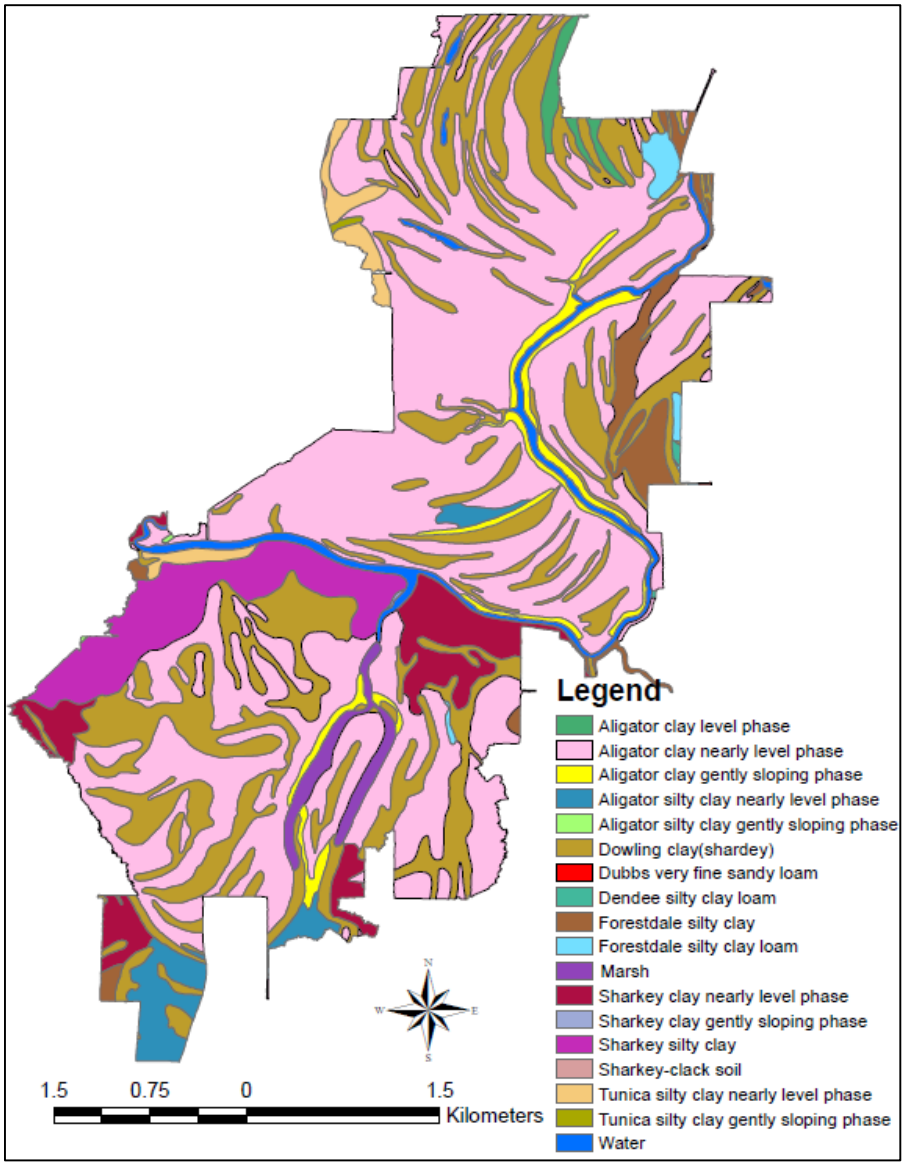

Figure 13: Soil map for Howden Lake watershed

5.2 Selection of the Sub-Watershed Covering Upstream Station Area

Fields are often connected to the streams and ditches with culverts for drainage, which are placed by farmers to convey accumulated water. The culverts often convey water from one sub-watershed to another. A site investigation was carried out to check the flow paths, the connection of the culverts and the small channel distributions in the watershed. The investigation was carried

out elaborately for the upstream station (HL1) area of the Howden Lake watershed. As the culverts (Figures 14 and 15) significantly affect the drainage flow pattern of the watershed, the location of the culverts were inspected visually during the field trip and incorporated into the numerical mesh for the overland flow simulation. A sub-watershed boundary was generated based on this site investigation for the upstream areas covering the watershed, and simulation was done accordingly. The sub-watershed area contributing the flow to the monitoring gage station 1 (HL1) is interested in this study, as indicated by a purple and closed curve (Figure 15). In this region of low relief, watersheds are of intensively cultivated fields drained by ditches and intermittently flowing streams or bayous. Because the watershed is very flat, it was difficult to determine the boundaries between sub-watersheds. For example, the runoff from one field may flow to more than one stream, and the watershed divide line can only be drawn based on the flow pattern during a simulation. The studied watershed controlled by an NSL gage was outlined in this way. The total area (including cultivated land, drainage ditches and a stream segment), perimeter and relief for the sub-watershed is shown in Table 5.

Figure 14: Culverts collecting water near the fields in the Howden Lake watershed

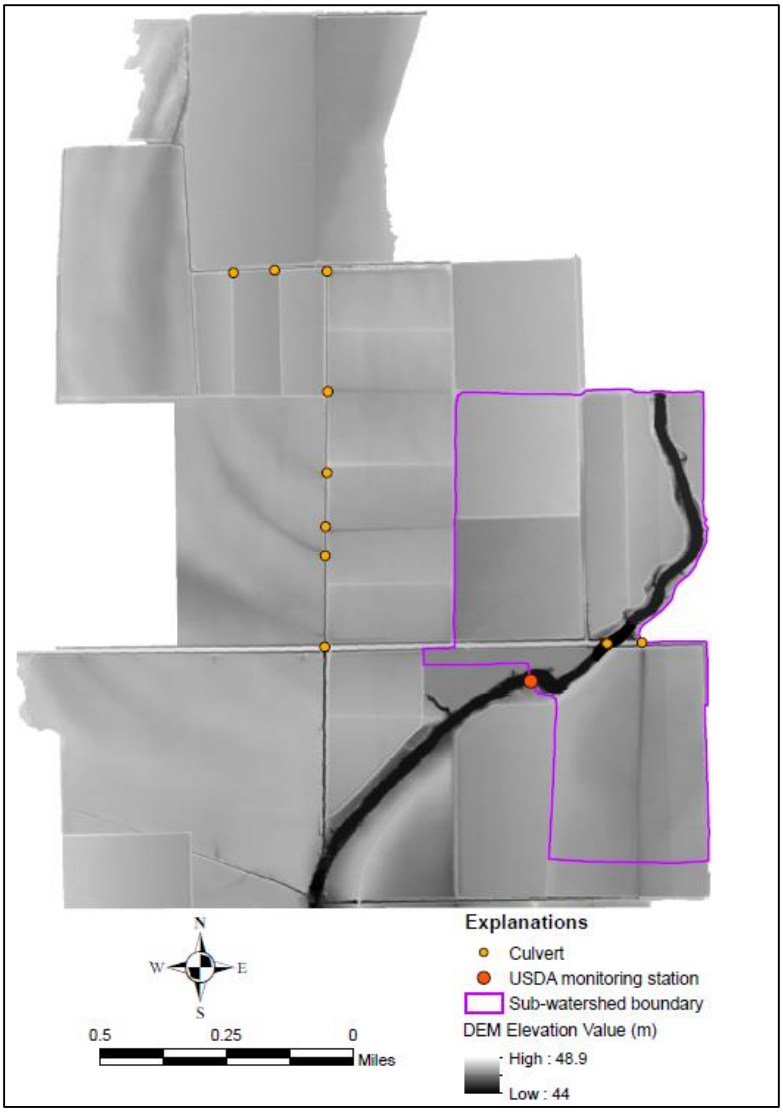

Figure 15: Identified Runoff Sub-watershed for the Station1 (HL1) showing in DEM

Table 5: Howden Lake Sub-watershed characteristics

Sub-Watershed perimeter (m)	**Sub-Watershed area (m^2)**	**Sub-Watershed relief (m)**	
		Max	**Min**
5066	973671	48.8	44.8

5.3 Mesh Generation

Detailed topographic data and mesh are necessary for accurate flow simulation. The 1.5 m resolution LiDAR topographic dataset (DEM) was used to generate the mesh using CCHE MESH generator for this watershed. A nearly uniform fine mesh (mesh spacing = 3.76 m ~ 4.98 m) was generated for the simulation (Figure 16). As the culverts significantly affect the natural drainage flow pattern of the watershed, the mesh was further refined near the culverts, ditches and small streams locally. The culverts were not simulated. They were represented by a small channel connecting the lands and the ditches (Figure 16). The mean mesh size is approximately 4 m and the smallest mesh size is approximately 1.5 m. Smoothing was applied to the initial bed to remove the noisy local irregularities.

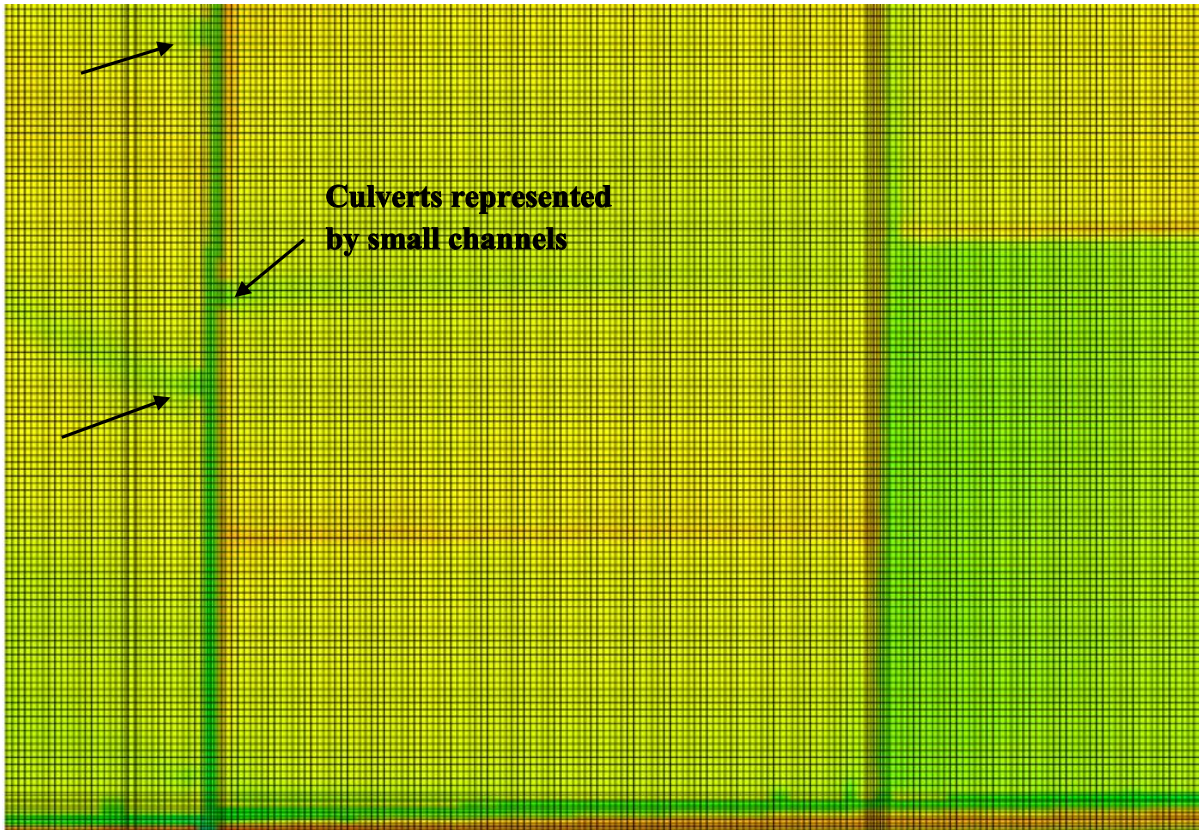

Figure 16: Identified Culverts showing in the CCHE mesh

5.4 Generation of Initial Condition Data

No discharge hydrograph was applied as a boundary condition for the watershed. Initial water surface elevation was set assuming the water depth was minimal (10^{-5} m). Many investigators assume a thin overland flow depth initially for simulating overland flow runoff (Liggett and Woolhiser, 1967, Govindaraju et al., 1990). This procedure will overcome the numerical difficulties at dried areas. The only boundary conditions imposed are three rating curves at the outlet boundary, which are located in the south part of the watershed indicated in Figure 18.

5.5 Generation of Distributed Manning's *n* Data

Manning's roughness coefficient (*n*) is a principal factor in the determination of runoff velocity and runoff distribution. Overland flow requires a Manning's roughness parameter for each grid or cell of the topography. One of the common ways to set Manning's *n* is to use LULC datasets. LULC data was downloaded from US Geologic Survey (USGS) (USGS, 2010) National Land Cover Dataset (NLCD). NLCD is Landsat-based, 30-meter resolution, land cover database. NLCD provides spatial reference and descriptive data for characteristics of the land surface. NLCD also provides land cover classification scheme based primarily on Landsat data along with numerous data types, such as topography, soil characteristics, census, agricultural statistics, wetlands, and other land cover maps. Using ERDAS imagine software, these land use layers were subset using the watershed boundary. The areas for different LULC of this watershed were also calculated. Figure 17 shows the LULC map (2010) for the entire Howden Lake watershed.

LULC distribution of 2010 is used for generating Manning's *n* value for the watershed. Manning's roughness coefficients for the land cover features for the channels and the floodplains

were obtained from published literature including Chow (1959), Kalyanapu et al. (2009), Graf (1998) and Henderson (1966). Using ERDAS Imagine software these published Manning's *n* values were adopted for each of the land use classes. According to the techniques Hossain et al., (2009) the Manning's *n* values were assigned using GIS and then LULC data were converted into the distributed Manning's *n* data. Table 6 shows the LULC classes and corresponding distributed Manning's *n* values.

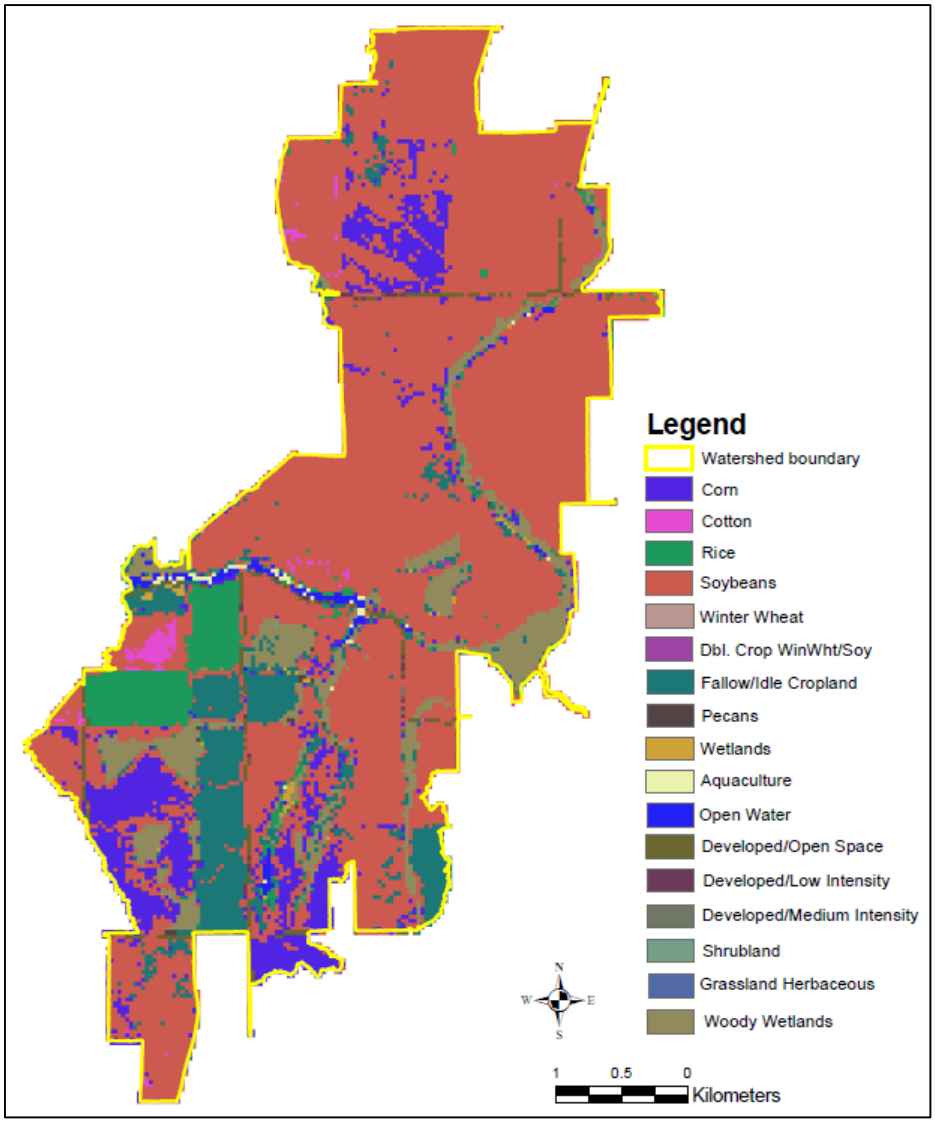

Figure 17: Land Use Land Cover map (2010) for Howden Lake watershed

Table 6: LULC distribution (2010) and Manning's *n* value for Howden Lake watershed

Code	Land cover	Count	Area (sq m)	Area (acres)	Description	Manning's *n*
1	Corn	1868	1681200	415.43	crop	0.035
2	Cotton	156	140400	34.69	crop	0.035
3	Rice	802	721800	178.36	crop	0.035
5	Soybeans	13336	12002400	2965.86	crop	0.035
24	Winter Wheat	2	1800	0.44	grains, hay,seeds	0.035
26	Dbl. Crop WinWht/Soy	16	14400	3.56	grains, hay,seeds	0.035
61	Fallow/Idle Cropland	1682	1513800	374.07	non-crop	0.025
74	Pecans	25	22500	5.56	crop	0.035
87	Wetlands	70	63000	15.57	other	0.11
92	Aquaculture	53	47700	11.79	other	0.05
111	Open Water	140	126000	31.14	NLCD-derived classes	0.025
121	Developed/Open Space	334	300600	74.28	NLCD-derived classes	0.016
122	Developed/Low Intensity	39	35100	8.67	NLCD-derived classes	0.03
123	Developed/Medium Intensity	5	4500	1.11	NLCD-derived classes	0.03
152	Shrubland	1	900	0.22	NLCD-derived classes	0.07
171	Grassland Herbaceous	1	900	0.22	NLCD-derived classes	0.05
190	Woody Wetlands	1604	1443600	356.72	NLCD-derived classes	0.16

The distributed Manning's *n* value (Table 6) for each of the land use classes was adopted using CCHE Graphical User Interface (GUI) for numerical simulation. From the LULC map it was found that this agricultural watershed mostly produces crops and grains such as soybean, corn, cotton and rice which have the Manning's *n* value of 0.035. There are many trees and bushes growing along the channel, so $n = 0.16$ was used for the channel and was kept unchanged for other rain event cases. A higher value of Manning's *n* (= 0.06) was assigned locally near the small channel joined with the main channel and also near the culvert areas. The three major land use categories and the corresponding surface roughness values of the sub-watershed of Howden Lake watershed were obtained from Table 6 and shown separately in Table 7. Figure 18 shows the Manning's *n* distribution for the sub-watershed.

Table 7**:** Three major surface roughness categories for sub-watershed

Roughness category	**Land cover**	**Manning's *n***
1	Crops (soybean, cotton, pasture and corn)	0.035
2	Open Water	0.025
3	Woody Wetlands	0.16

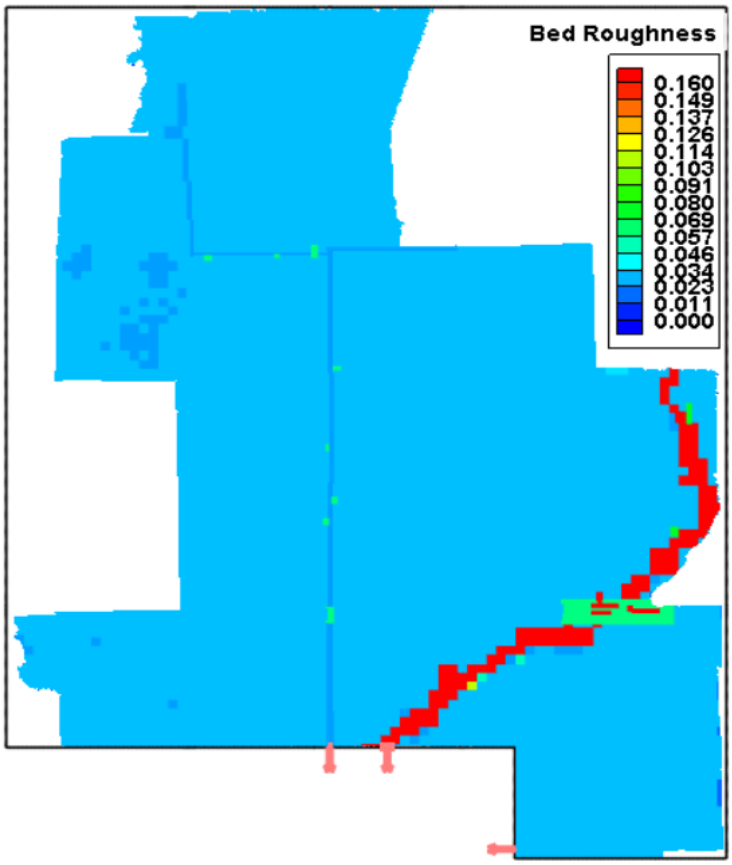

Figure 18: Manning's *n* distribution showing in CCHE GUI.

5.6 Sensitivity to Manning's *n* Analysis

Manning's *n* is dependent on the surface irregularity, surface granular structure, vegetation type and density etc. (Arcement and Schneider, 1990; Vieux, 2001; Jain et al., 2004; Barnes, 1967;

Aldridge and Garrett, 1973). As selecting appropriate Manning's *n* is very important for the runoff simulation, sensitivity analyses have been conducted by many authors. Jaber and Mohtar (2003) conducted sensitivity analysis using Manning's roughness coefficient, watershed slope, and excess rainfall rate in order to test the accuracy of their numerical scheme. The sensitivity of the 2D shallow water model results to bed friction has also been studied by Cea et al. (2008) and Morgali and Linsley (1965). The sensitivity of the CCHE2D numerical results for Howden Lake watershed to Manning's *n* was also examined using the values of 0.030, 0.035, 0.08, 0.17, 0.2, and 0.3 $m^{-1/3}s$ for the entire cropland area except channels and open water. From Figure 19 it can be seen that smaller Manning's *n* values result in the higher runoff peak discharge and earlier peak flow time. An increase in the bed friction coefficient diminishes considerably the peak discharge, delaying its time of arrival.

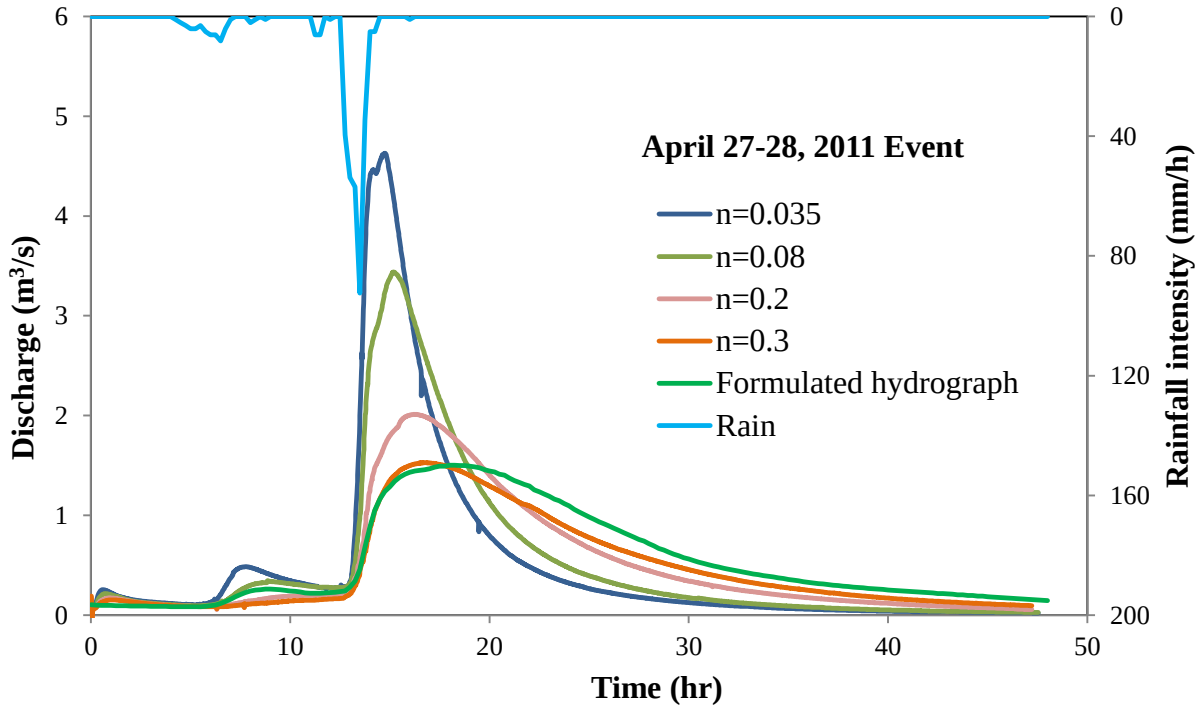

Figure 19: Simulation results using different Manning's *n*

A visual comparison of discharge hydrographs based on stage measurements and numerical simulation (Figure 19) indicates that n = 0.2 to 0.3 (Kalyanapu et al., 2009; Singh et al., 2014) is the most appropriate choice for the cropland area. The peak times of the measured and simulated runoffs are consistent for the value of n = 0.3. These values are significantly higher than those in Table 6. It should be noted that the water depth of runoffs is very small in comparison to any physical roughness of the cultivated watershed area. The actual forcing on the runoff is more than just the bed shear stress represented by the Manning's equation; drag forces in the horizontal direction and even the surface tension may become significant. Therefore, the effective Manning's roughness coefficients should be much larger. Vegetation density and thickness of the micro plant effect during different season of the year were not considered separately for the runoff simulation of the watershed.

A rainfall event on April 27-28, 2011 was used for sensitivity analysis of Manning's roughness coefficient. Using Manning's n = 0.3, the total observed rainfall volume for the April 27-28, 2011 event (Figure 19) was approximately 86,000 m^3. The total simulated runoff volume was slightly less which is 80,600 m^3; this is reasonable because the runoff can tail a long time but the simulation is stopped earlier at 47 hr. There were several small rain events that occurred before the event shown in Figure 19, the runoff information in the observed water surface elevation may have been influenced by the earlier activities.

5.7 Calibration and Validation to Largest Observed Rainfall

Five historic and large rain events provided by NSL were selected for the model application. Among these, three major rainfall events were in the year of 2011 and the others were

in 2013. To avoid the error due to evaporation, soil wetting and infiltration, etc., only these five large rain events were considered.

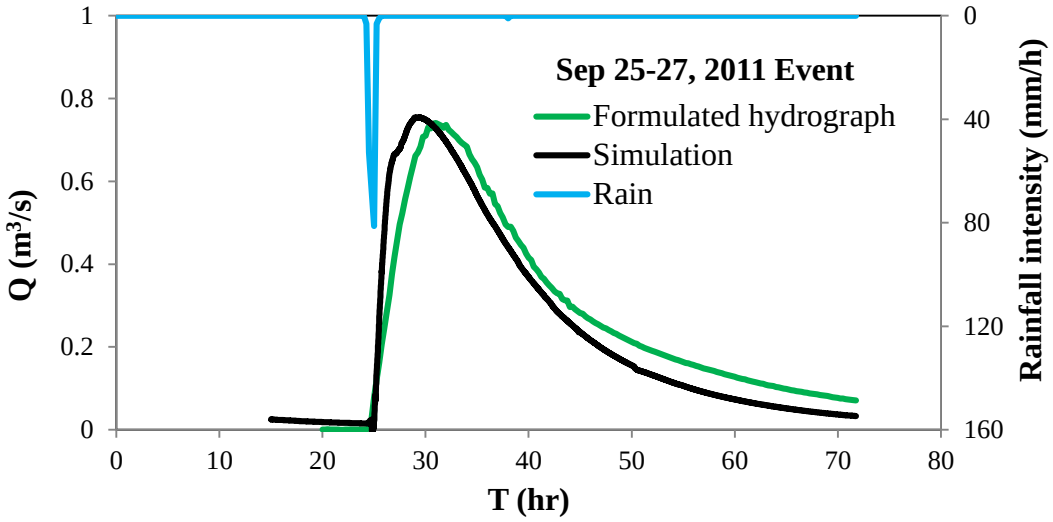

(a)

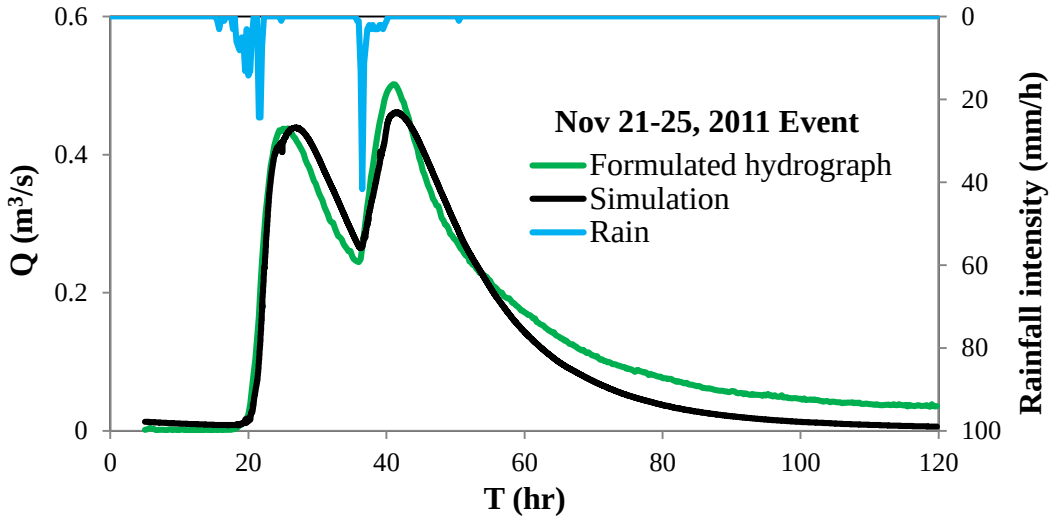

(b)

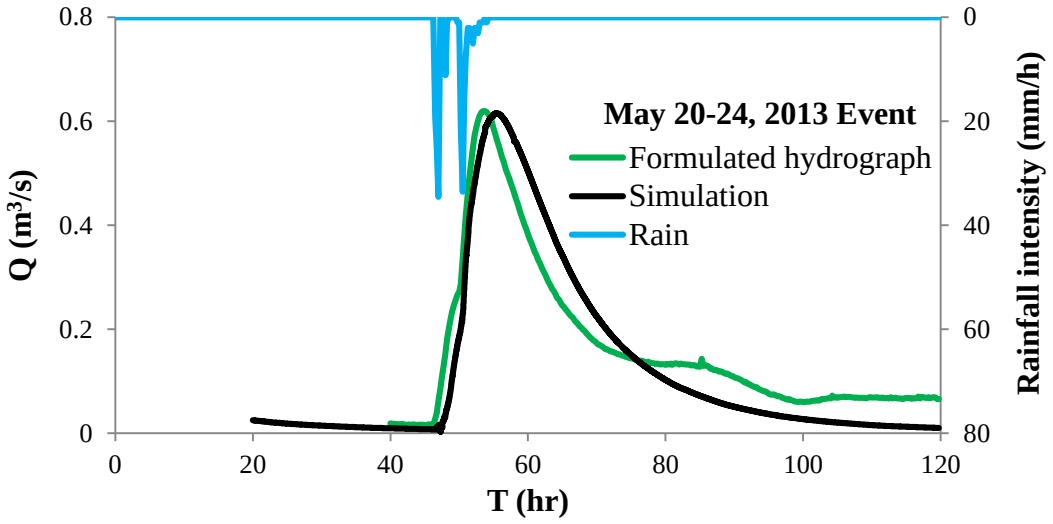

(c)

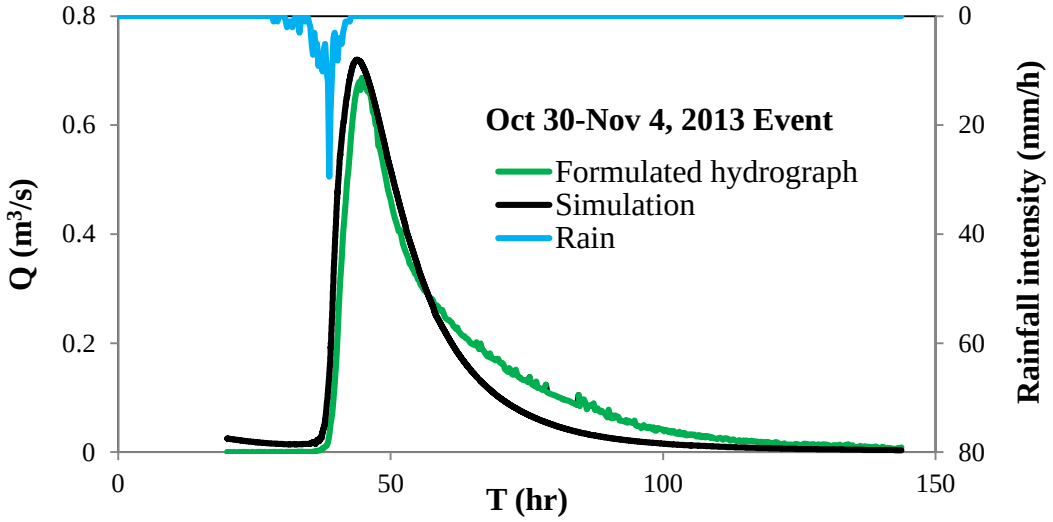

(d)

Figure 20. Comparisons of simulated runoff and Formulated hydrograph (Equation 25).

Figure 20 compares several additional runoff events and numerical simulations. All simulations applied the same calibrated Manning's coefficient, n = 0.3. The only variable changed in the CCHE2D model input was the rainfall distribution for all data sets. The simulated

hydrographs fit well with those computed from Equation 25 shown below. The two rain peaks of the 5/2011 event were separated by 2 hours approximately, but those of the 11/2011 event were separated by 15 hours. The runoff of the 5/2011 event showed only one peak because the two rain peaks were very close, and the runoff response had a delay and smoothed out the double peak feature. However, the time interval between the two peaks of the 11/2011 event was much longer, so the hydrologic response also displayed two peaks. These watershed responses are reproduced by the numerical simulations.

To compare the measured and simulated flow discharge hydrograph a rating curve of the form

$$Q = y(L - L_0)^z \tag{25}$$

was developed (Figure 19 and 20), in which L is the measured water surface elevation, y and z are parameters identified by trial and error, and L_0 is the water surface elevation at which the runoff starts after a rain. All the parameters of the equation are listed in Table 8.

Table 8. Parameters of selected runoff events for numerical simulations

Event	Rainfall depth (mm)	Volume*(m^3)	z	y	L_0 (m)
4/27-4/28/2011	88.39	85817	2.4	1.223	0.45
9/25-27/2011	52.32	50946	1.8	5.211	0.48
11/21-25/2011	62.99	61333	1.4	1.613	0.45
5/20-24/2013	48.77	47483	1	1.436	0.59
10/30-11/4/2013	53.59	52182	1.9	4.24	0.78

*Computed from the main bulk of the rain event.

Because the channel was used by farmers as a water storage pond seasonally, the water surface elevation L_0 varied independently of antecedent precipitation. Parameters y and z were

determined using the total volume of each rain. Attempts were made to fit all simulated curves using unified *y*, *z* and a general base stage L_0, but the result showed much larger discrepancies between the formula and the simulations. The difficulty of obtaining unified *y* and *z* may be due to the human activity induced variation of L_0 which affected the calibration level of the formulation randomly. The differences of L_0 in Table 8 for these events are up to 0.33m which introduced significant and systematic disturbances between the data for each hydrologic event. This may be why the rating curve can be fitted well only for individual events.

5.8 Model Performance Evaluation

Model accuracy was assessed by using the statistical technique (*NSE*). Nash-Sutcliffe efficiency is a normalized statistic that determines the relative magnitude of the residual variance ('noise') compared to the measured data variance ('information') (Nash and Sutcliffe, 1970). *NSE* is computed as:

$$NSE = 1 - \frac{\sum_{i=1}^{n} (O_i - S_i)^2}{\sum_{i=1}^{n} (O_i - \bar{O})^2} \tag{26}$$

where O_i = *i*th observation value for the constituent being evaluated, S_i = *i*th simulated value for the constituent being evaluated, $\bar{O}$ = mean of observed data for the constituent being evaluated, and *n* is the total number of observations. The range of *NSE* lies between 1.0 (perfect fit) and $-\infty$. Values between 0.0 and 1.0 are generally viewed as acceptable levels of performance, whereas values $\leq$ 0.0 indicates that the mean observed value is a better predictor than the simulated value, which indicates unacceptable performance (Moriasi et al. 2007). The values of Nash-Sutcliffe

efficiency *NSE* for discharge (Table 9) for all of the five rain storms are in very good range (Moriasi et al. 2007). These quantitative parameters and visual comparison of the simulated discharge and the formulated hydrograph (observations) show that the model simulated all the events to a reasonably good accuracy.

Table 9. Model evaluation statistics for surface runoff using NSE

Rain Event	NSE	Performance Rating
4/27-4/28/2011	0.95	Very good
9/25-27/2011	0.90	Very good
11/21-25/2011	0.95	Very good
5/20-24/2013	0.83	Very good
10/30-11/4/2013	0.91	Very good

5.9 Overland Flow Simulation Results

The watershed has multiple ditches between fields, discharging runoff from the lands into a stream channel (Figure 15, 21). The ditches in the watershed are connected to the stream. The monitoring gage was set at the downstream of the channel (Figure 22 and 23) or the outlet of the watershed. The flow in the ditch and stream channels during these events was simulated together with the runoff.

(a) (b)

Figure 21: Site investigation in the watershed near station 1 showing (a) Ditch and (b) tillage rill over one of the surveyed agricultural lands

Figure 24 shows the simulated vector direction fields (a, c), water depth distribution (b) and the contours of the land topography (d) of a small simulation area (dashed rectangle area in Figure 23) for the April 2011 rainfall event (Table 8). The bed elevation of this area ranges from 47.4m to 46.8m approximately. Figure 24a shows the vector directions near the end of the simulation when the runoff is weak. Although the variation of the bed surface topography is very small, the simulation shows how the runoff is controlled by micro-topography (Figure 24b). Figures 24c and 24 d show the vector direction field and water depth at the peak time of the rainfall.

The overall water depth is much deeper at this time because of the rainfall intensity, and the flow directions are less affected by the local micro-topographic features. The flow on the right side of the domain (Figure 24 c and 24 d) is still runoff, but it becomes free surface flow on the left with the water depth more than 0.2 m.

Figure 22. USDA monitoring station shown in Figure 23 (picture taken during the site investigation)

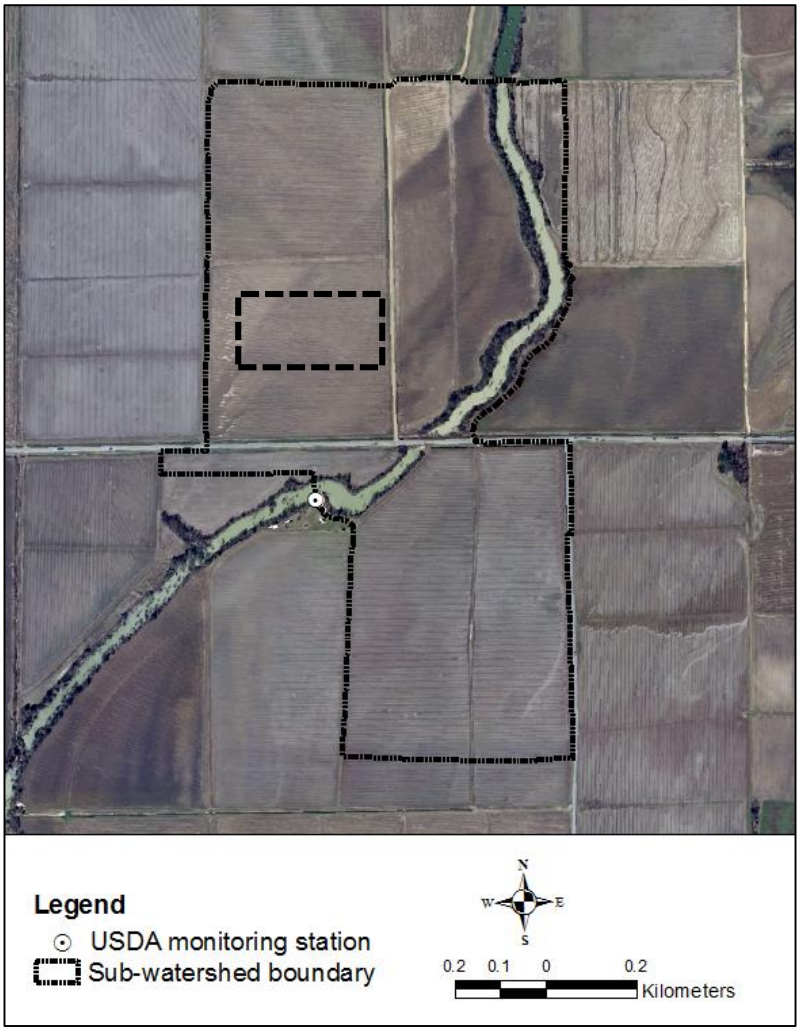

Figure 23. Identified watershed for the runoff gage location. Simulated runoff vectors and bed elevation contours of the rectangle area (black thick dashed line) are shown in Figure 24.

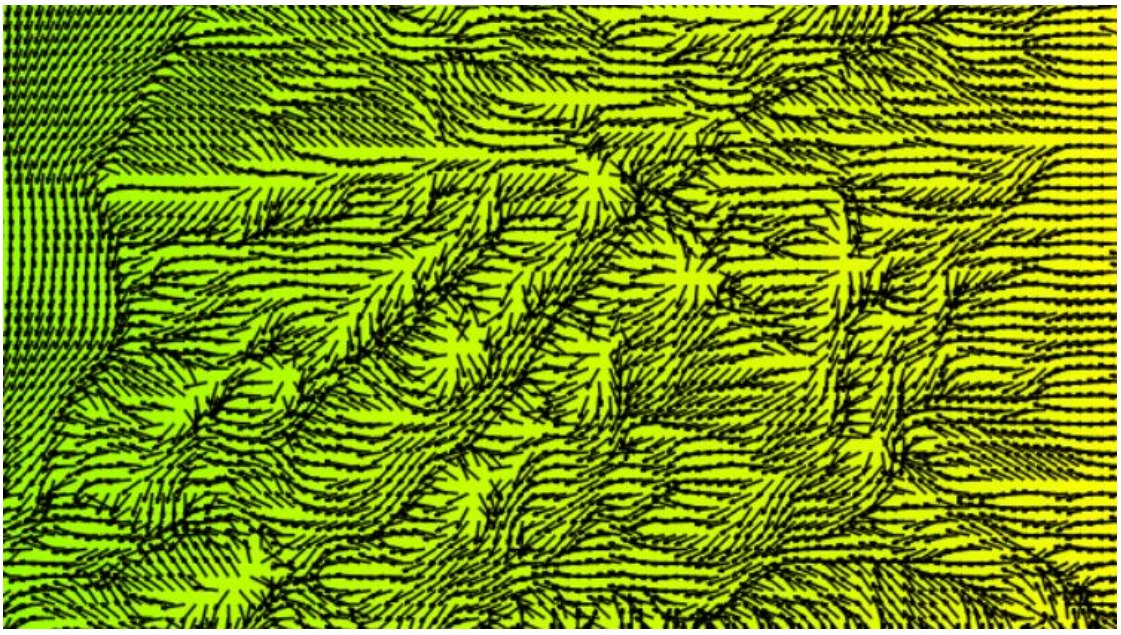

(a)

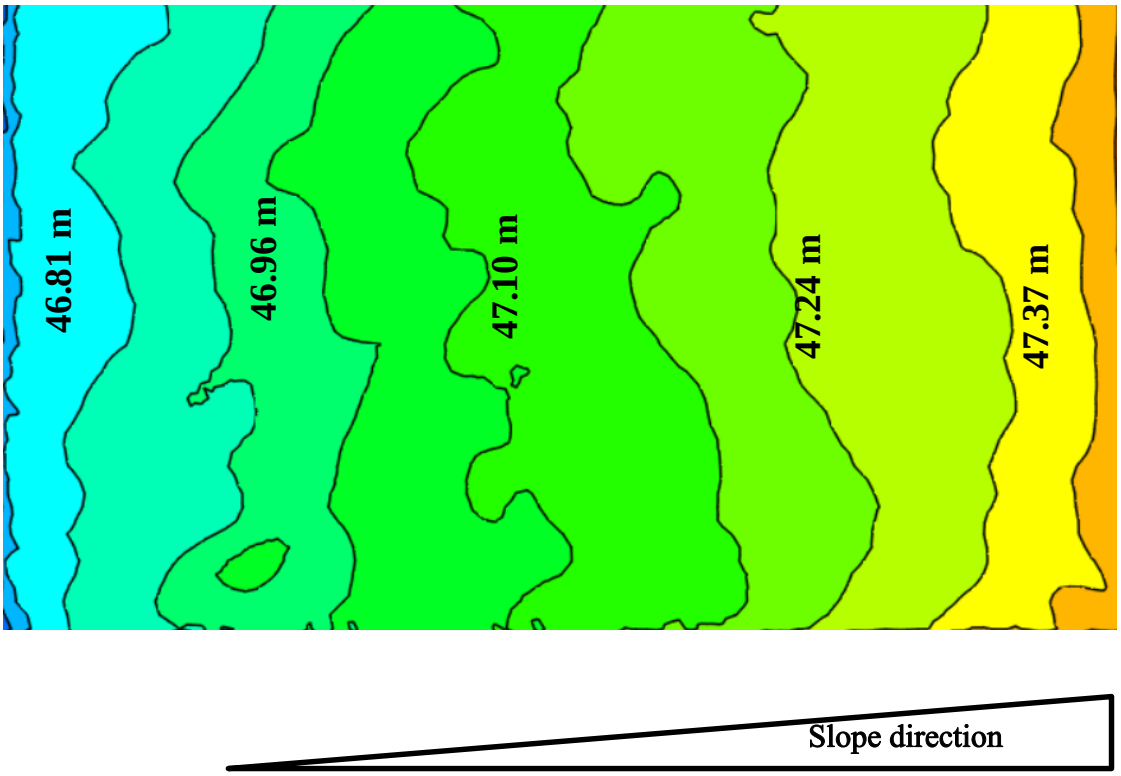

(b)

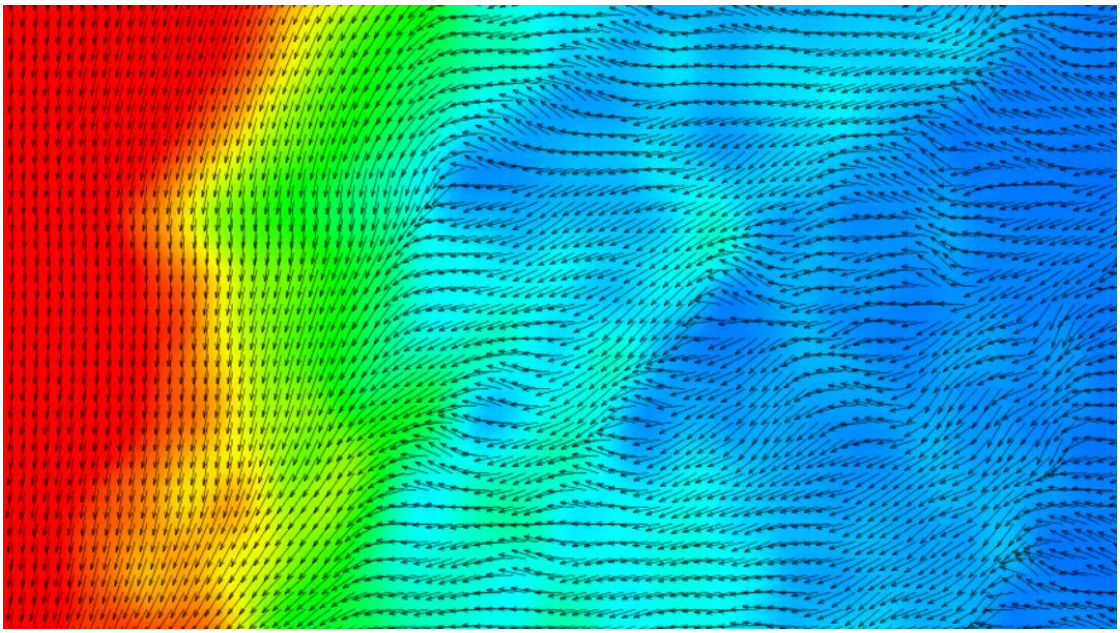

(c)

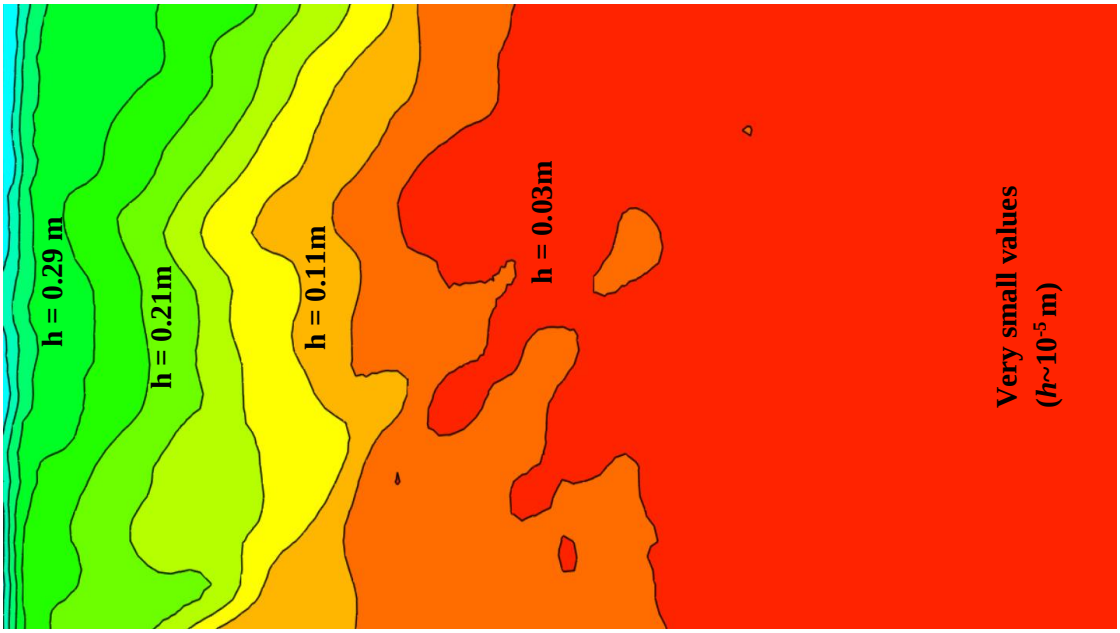

(d)

Figure 24. (a)Velocity direction distribution and (b) Bed elevation contours of this area near the end of the simulation; (c) Velocity direction and (d) the water depth distribution at the peak of the April 2011 rainfall. The area is indicated in Figure 23 using a dashed rectangle.

Larger channels that drain the watershed are bayous that contain water at all times, but are stagnant between runoff events. Discharge occurs only following rainfall, which may occur as intense thunderstorms or low-intensity events associated with major frontal movements. The latter type of events may stretch over several days of drizzle and sporadic showers. During growing seasons, channels experience some flow and stage fluctuation due to irrigation withdrawals and return flows. Figure 25 shows the simulated flows in the channel network of the watershed. The contours represent the distribution of the unit flow discharge. The vectors in the ditches and the stream formed a network indicated by the large velocity vectors; those in the runoff area are too small to be seen. The simulated results in the channel were not validated because no velocity data were taken in the channel. The advantage of this model for runoff prediction is that it provides not only the hydrograph, but also the temporal and spatial distribution of the water depth and flow velocity, which can be used for studying soil erosion, agro-pollutant transport and water quality.

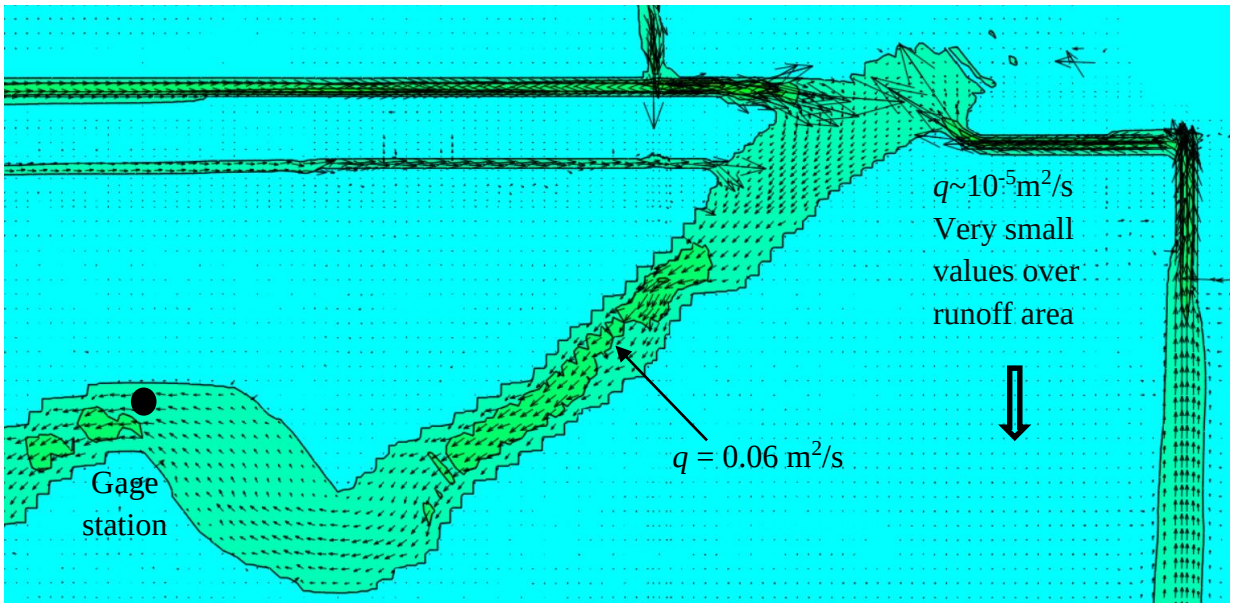

Figure 25. Simulated flow in the network of irrigation channels and the stream channel in the watershed

CHAPTER 6

CONCLUSIONS AND RECOMMENDATIONS

6.1 Conclusions

The numerical model CCHE2D was applied to model runoff from watersheds large and complex enough to include both overland and channel flow processes. The model was verified and validated using both analytical solutions and experimental data, and applied to a real world watershed. Good agreements between the analytical solutions, experimental data, and numerical simulations were obtained. For the experimental cases with a complex shaped watershed, the numerical model has the ability to model runoff over the slope surfaces and the channel flows.

The model was set up and applied to a more complex, real world scenarios of an agricultural watershed in the Mississippi River alluvial plain, and reasonable results were obtained. Several observed rain events were selected for the model application. To avoid errors due to losses of water by evaporation, soil wetting and infiltration, etc., only large rain events were considered. Because of human activities, particularly the stage variations of the water stored in the channel, it is difficult to derive a unified rating curve applicable for all of the observed runoffs. The sensitivity of the model to bed friction was studied. An increase in the bed surface friction coefficient diminishes considerably the peak runoff discharge, delaying its time of arrival. Values of n = 0.2~0.3 were found to be adequate for the runoff simulation in the studied watershed. Statistical performance analyses were employed to evaluate the modeled results. The visual comparison and

the statistical analyses of the simulated runoff hydrographs and the observed runoffs show that the model simulated all the rainfall events with a reasonable accuracy. With a high resolution mesh, the overall performance of the model in the real field application cases can be termed as satisfactory and the present model can be used for simulation of rainfall-generated runoff in agricultural watersheds. The ditch and stream channels in the domain are a connected channel network of free surface flows. The model is able to simulate the runoff, free surface flow and their transitions seamlessly. This capability of this model can be implemented for soil and water conservation studies and can be utilized for the watershed Best Management Practice (BMP) design. The model would be also useful for studies related to top soil erosion and agro-pollutant transport. Additional work is needed to further extend the research toward these areas.

6.2 Recommendations for Future Study

The followings are recommended for future studies to improve the current work:

- This numerical runoff model can be combined with the sediment transport model for the top soil erosion study. This model can also be combined with the water quality modeling to study the pollutant transport in runoff.
- To simplify the analysis and procedure of the model verification and validation, infiltration was not included in this study. The model can be improved by incorporating the infiltration process which will help to understand the areas runoff process more accurately when infiltration is significant.
- The model has been applied to only one field study. Further validation of the new watershed areas with actual data is needed for different types of areas such as urban, residential etc.

BIBLIOGRAPHY

Abbott, M.B., 1966, An introduction to the Method of Characteristics, Elsevier, New York.

Aldridge, B. N., and Garrett, J. M.,1973, Roughness coefficients for stream channels in Arizona. U. S. Geological Survey, Open File Report, Tucson, AZ.

Arcement, G. and Schneider, V.,1990, Guide for selecting Manning's roughness coefficients for natural channels and flood plains, U. S. Geological Survey Water-Supply Paper 2339.

Barnes, H. H., Jr., 1967, Roughness characteristics of natural channels, U.S. Geological Survey Water Supply Paper 1849, p. 213

Bates, P.D., Horritt, M., Smith, C., Mason, D., 1997, Integrating remote sensing observations of flood hydrology and hydraulic modelling, Hydrological Processes 11, pp. 1777–1795.

Bates, P.D. and Roo, A.P.J., 2000, A simple raster-based model for flood inundation simulation, Journal of Hydrology, 236, pp. 54-77.

Book, D.E., J.W. Labadie, and D.M. Morrow, 1982, Dynamic vs. Kinematic Routing in Modeling Urban Storm Drainage. In Urban Stormwater Hydraulics and Hydrology, B.C. Yen (ed.), Proceedings of the Second International Conference on Urban Stormwater Drainage, pp. 154-163.

Cea, L., Puertas, J., Pena, L., and Garrido, M., 2008, Hydrologic forecasting of fast flood events in small catchments with a 2D-SWE model. Numerical model and experimental validation. In: World Water Congress 2008, 1–4 September 2008, Montpellier, France.

Cea, L., Garrido, M. and Puertas, J., 2010, Experimental validation of two-dimensional depth-averaged models for forecasting rainfall-runoff from precipitation data in urban areas, Journal of Hydrology, March 2010, Vol. 382, pp. 88-102.

Chow V.T., 1959, Open-channel Hydraulics, New York, McGraw-Hill Book Company, 680p.

Chow V.T., Maidment D.R., and Mays L.W., 1988, Applied hydrology, McGraw-Hill Book Company, 1988.

Cooley, R.L. and Moin, S. A., 1976, Finite element solution of Saint-Venant equations, ASCE J. Hudraul Div., 102, pp. 759-775.

Costabile, P., Costanzo, C., Macchione F. and Mercogliano, P., 2012, Two-dimensional model for overland flow simulations: A case study, European Water, 38, pp. 13-23.

Cundy, T.W., Tento, S.W., 1985, Solution to the kinematic wave approach to overland flow routing with rainfall excess given by the Philip equation. Water Resources Research 21, pp. 1132-1140.

Du J.K., X. Shunping, Youpeng X., Xu C., and Singh V.P., 2007, Development and testing of a simple physically- based distributed rainfall- runoff model for storm runoff simulation in humid forested basins. Journal of Hydrology, 336, pp. 334-346.

Esteves, M., Faucher, X., Galle, S. and Vauclin, M., 2000, Overland flow and infiltration modeling for small plots unsteady rain: numerical results versus observed values, Journal of Hydrology, 228, pp. 265-282.

Fread, D. L., 1985, Channel routing, In: Hydrological Forecasting, M. G. Anderson and T. P. Burt (Ed.), Wiley, New York.

Fisk, H.N., 1944, Geological investigations of the alluvial valley of the lower Mississippi River: Vicksburg, Mississippi, U.S. Army Corps of Engineers, Mississippi River Commission, 78 p.

Freeze, R.A., 1978. Mathematical models of hillslope hydrology. In: Kirkby, M.J., (Ed.), Hillslope hydrology, Wiley Interscience, New York, pp. 177–225.

Gottardi G., and Vinutelli M., 2008, An accurate time integration method for simplified overland flow models, Advances in Water Resources, Vol 31, pp. 173-180.

Govindaraju RS, Kavvas ML, Jones SE., 1990, Approximate analytical solutions for overland flows. Water Resources Research, 26 (12), pp. 2903-2012.

Graf W. H., 1998, Hydraulics of Sediment Transport, Water Resources Publications LLC, 513p.

Haile A. T. and Rientjes T.H.M., 2005, Effects of LiDAR DEM resolution in Flood Modelling: A model sensitivity study for the city of Tegucigalpa, Hondurus, ISPRS WG III/3, III/4, V/3 Workshop "Laser scanning 2005", Enschede, the Netherlands, September 12-14, 2005.

Henderson F. H. and Wooding R. A.,1964, Overland flow and groundwater flow from a steady rainfall of finite duration, Journal of Geophysical Research, Vol. 69 (8), pp. 1531-1540.

Henderson F. H., 1966, Open-channel flow, New York, MacMillan Publishing Co., Inc., 522p.

Howes, D.A., Abrahams, A.D., Pitman, E.B., 2006, One- and two-dimensional modelling of overland flow in semiarid shrubland, Jornada basin, New Mexico. Hydrol. Process. 20, pp. 1027-1046.

Hossain, AKM A., Jia Y. and Chao X., 2009, Estimation of manning's roughness coefficient distribution for hydrodynamic model using remotely sensed land cover features, 17th International Conference on Geoinformatics, Fairfax, VA: George Mason University, 2009.

Iwagaki, Y., 1955, Fundamental studies on the runoff analysis by characteristics, Kyoto University Disaster Prevention Res. Inst., Japan, Bull., Bulletin 10, pp. 1-25.

Jabar FH, Mohtar RH, 2003, Staility and accuracy of two-dimensional kinematic wave overland flow modeling, Advances in Water Resources, 26, pp. 1189-1198.

Jain, M. K., Kothyari, U. C., and Raju, K. G. R., 2004, A GIS based distributed rainfall-runoff model, Journal of Hydrology, 299, pp. 107-135.

Jia, Y., and Wang, S.S.Y., 1999, Numerical model for channel flow and morphological change studies, ASCE, Journal of Hydraulic Engineering, Vol. 125, No. 9, pp. 924-933.

Jia, Y., Wang, S. S. Y., and Xu, Y. C., 2002, Validation and application of a 2D model to channel with complex geometry, Int. J. Comput. Eng. Sci., 3(1), pp. 57-71.

Jia, Y., X.B. Chao, Y.X. Zhang and T.T. Zhu, 2013 Technical Manual of CCHE2D, V4.1, NCCHE-TR-02-2013, the University of Mississippi.

Kalyanapu A. J., Burian S. J. and McPherson T. N., 2009, Effect of land use-based surface roughness on hydrologic model output, Journal of Spatial Hydrology, 9(2), Fall 2009.

Kivva, S.L., Zheleznyak, M.J., 2005, Two-dimensional modeling of rainfall runoff and sediment transport in small catchments areas. Int. J. Fluid Mech. Res. 32 (6), pp. 703-716.

de Lima J.L,M.P., Singh V.P., 2002, The influence of the pattern of moving rainstorms on overland flow, Advances in Water Resources, 25, pp. 817-828.

Liggett, J. A., and Woolhiser, D. A., 1967, Difference solutions of the shallow water equations, J. Engrg. Mech. Div., ASCE, 93(2), pp. 39-71.

Liu Q.Q., Chen L., Li J.C., and Singh V.P., 2004, Two-dimensional kinematic wave model of overland-flow, Journal of Hydrology, 291(1-2), pp. 28-41.

Marks, K., and Bates, P., 2000, Integration of high-resolution topographic data with floodplain models. Hydrologic processes, 14, pp. 2109-2122.

Morgali, J.R., and Linsley, R.K., 1965, Computer analysis of overland flow. J. Hydrol. Div. Proc. American Society of Civil Engineers. HY3, pp. 81-100.

Moriasi, D. N., Arnold, J. G., Van Liew, M. W., Bingner, R. L., Harmel, R. D., and Veith, T. L., 2007, Model evaluation guidelines for systematic quantification of accuracy in watershed simulations." Trans. ASABE, Vol. 50(3), pp. 885-900.

Morris, E. M., and Woolhiser, D. A., 1980, Unsteady one-dimensional flow-over a plane: Partial equilibrium and recession hydrographs, Water Resources Research, Vol. 16 (2), pp. 355-360.

Nash, J. E., and Sutcliffe J. V., 1970, River flow forecasting through conceptual models: Part 1. A discussion of principles. Journal of Hydrology, Vol. 10 (3), pp. 282-290.

Nunoz-Carpena, R., Miller, C.T., and Parsons,J.E., 1993, A quadratic Petrov-Galerkin solution for kinematic wave overland flow, Water Resources Research, Vol.29(8) pp. 2615-2627.

Remson, R. D., Hornberger, G.M., and Molz, F. J., 1971, Numerical Methods in Subsurface Hydrology, Willey Interscience, New York.

Rousseau M., Cerdan, O., Delestre, O. Dupros F., James, F. and Cordier S., 2012, Overland flow modelling with the shallow water equation using a well-balanced numerical scheme: Adding efficiency or just more complexity? https://hal.archives-ouvertes.fr/hall-00664535.

Singh J., Altinakar, M.S., Ding, Y., 2014, Numerical Modeling of Rainfall-Generated Overland Flow Using Nonlinear Shallow-Water Equations, Journal of Hydrologic Engineering, 10. .1061/(ASCE)HE.1943-5584.

Singh, V. P., 1983, Analytical solutions of kinematic equations for erosion on a plane II. Rainfall of finite duration, Advances in Water Resources, Vol. 6 (2), pp. 88-95.

Singh, V. P. and Regl, R.R., 1981, Analytical solutions of kinematic equations for erosion on a plane I. Rainfall of indefinite duration, Advances in Water Resources, Vol. 6 (1), pp. 2-10.

Singh, V. P., 1996, Kinematic wave modeling in water resources: surface water hydrology, Chichester: John Wiley and Sons Ltd; 1996.

Singh V.P., 2001, Kinematic wave modelling in water resources: a historical perspective. Hydrological Processes, 15(4), pp. 671-706.

Singh V.P., 2002, Is hydrology kinematic? Hydrological Processes, 16(3), pp. 667-716.

Szymkiewicz, R., 1991, Finite-element method for the solution of the Saint Venant equations in an open channel network, Journal of Hydrology, 122, pp. 275-287.

Szymkiewicz, R. and Gasiorowski, D., 2012, Simulation of unsteady flow over floodplain using the diffusive wave equation and the modified finite element method, Journal of Hydrology, 464, pp. 165-175.

Unami, K., Kawachi, T. Kranjac-Berisavljevic, G., Abagail, F. K., Maeda, S. and Takeuchi, J. 2009, Case Study: Hydraulic Modeling of Runoff Processes in Ghanaian Inland Valleys, J. Hydraul. Eng., 135 (7), pp. 539-553.

U. S. Geological Survey (USGS), 2010, "Seamless data distribution system" http://seamless.usgs.gov/.

Venkata, R.K., Eldho, T.I., and Rao, E.P., 2009, A diffusion wave based integrated FEM-GIS model for runoff simulation of small watersheds, J. Water Resource and Protection, 2009**,** 1, 391-399 doi:10.4236/jwarp.2009.16047 Published Online December 2009.

Vieux, B. E. (2001). Distributed hydrologic modeling using GIS, Kluwer Academic Publishers, Dordrecht, The Netherlands.

Woolhiser, D.A., Liggett, J.A., 1967, Unsteady, one dimensional flow over a plane-The rising hydrograph. Water Resources Research 3 (3), pp. 753-771.

Zhang, W., and Cundy, T.W., 1989, Modeling of two-dimensional overland flow, Water Resources Research, Vol. 25, No 9, pp. 2019-2035.

VITA

EDUCATION

- M.S. in Engineering Science (Anticipated in Spring 2016)
  Emphasis: Computational Hydroscience
  National Center for Computational Hydroscience and Engineering (NCCHE), The University of Mississippi, MS, USA
  2009-2016
  Advisor: Dr. Yafei Jia
- MS in Geology
  University of Mississippi, MS, USA
  2006-2010
  Advisor: Dr. Greg Easson
- MS in Geological Science
  Jahangirnagar University, Bangladesh
  1997-2000
  Advisor: Dr. Khairul Bashar
- Bachelor in Geological Science
  Jahangirnagar University, Bangladesh
  1993-1996

AWARDS AND SCHOLARSHIPS

- Graduate Student Council Research Symposium Best Poster Award in Engineering Sciences, 2011, The University of Mississippi
- United States Department of Agriculture (USDA) - National Sedimentation Laboratory (NSL) research grant
- School of Engineering Thesis fellowship
- National Center for Computational Hydroscience and Engineering (NCCHE) graduate research assistantship
- University of Mississippi Geoinformatics Center (UMGC) graduate research assistantship
- Department of Geology and Geological Engineering, The University of Mississippi teaching assistantship
- University Scholarship, Jahangirnagar University, Savar, Dhaka

PUBLICATIONS

Shirmeen T., Jia Y., Locke M. A. Lizotte R. and Shields F.D., 2016, Numerical Modeling of Rain Induced Overland and Channel Flows, *Journal of Hydrologic Engineering*, Under Review.

Shirmeen T., Jia Y., Locke M. A. Lizotte R., 2015, Numerical Modeling of Rain induced Overland Flows, *World Environmental & Water Resources Congress (EWRI) 2015*: Floods, Droughts, and Ecosystems, ASCE 2015.

Shirmeen T. and Jia Y., 2015, Rain Induced Runoff Simulation in an Agricultural Watershed, *Graduate Student Council Research Symposium 2015*, The University of Mississippi, podium presentation.

Jia, Y., Shirmeen, T., Hossain, A., and Zhang, Y., 2013, Dam Break Flood Simulation and Consequence Analyses Using CCHE2D, *12th International Benchmark Workshop on Numerical Analysis of Dams*, 2nd - 4th October 2013, Graz –Austria, poster presentation.

Shirmeen T., Jia Y., Hossain A., Altinakar M., Wilcox D., Locke M., and Lizotte R., 2013, Watershed Delineation in the Deltaic Areas of North West Mississippi Using LIDAR Data, *MAESC 2013 Conference*, The University of Mississippi, Oxford MS, Oct 28-29, 2013.

Shirmeen T. and Jia Y., 2013, Modeling Rainfall Runoff using 2D Shallow Water Equation, *Mississippi Water Resources Conference*, April 2-3, 2013, Hilton Jackson, Jackson, MS.

Shirmeen T., Jia Y., Hossain A. and Chao X., 2011, GIS of National Response Center's (NRC) Chemical Incident Database, *MAESC 2011 Conference*, Christian Brothers University, Memphis, TN.

Shirmeen T. and Easson G., 2011, Impervious Surface Mapping using High Resolution Satellite Imagery, *Graduate Student Council Research Symposium 2011*, The University of Mississippi, poster presentation.

Shirmeen, T. and Easson, G., 2008, Storm Water Runoff: Effects of Changes in Impervious Surfaces, IGARSS 2008, Boston, MA.

Shirmeen, T. Robinson H., and Easson, G., 2008, Classification of Oxford City Road Intersections Based on Available Police Accident Data, *Graduate Student Council Research Symposium 2008*, The University of Mississippi, poster presentation.

Shirmeen, T. and Bashar, K., 2000, Hydrogeology of Lakshmipur Sadar Upazila, Lakshmipur District, Bangladesh. *Bangladesh Geoscience Journal*, Vol. 6, P. 153-162.

Bashar, K. and Shirmeen, T., 2000, Groundwater Quality of Lakshmipur Sadar Upazila, Lakshmipur District, Bangladesh. *Bangladesh Geoscience Journal*, Vol. 6, P. 163-175.